

Research on Engineering Structures & Materials



www.jresm.org



Prediction of the flexural capacity of steel fiber reinforced self-compacting concrete beams combining neural networks, the Barcelona test and the gravitational search algorithm

David Cotes-Prieto, Luis Zapata-Ordúz

Online Publication Date: 30 January 2025

URL: http://www.jresm.org/archive/resm2025-569ml1208rs.html

DOI: http://dx.doi.org/10.17515/resm2025-569ml1208rs

Journal Abbreviation: Res. Eng. Struct. Mater.

To cite this article

Cotes-Prieto D, Zapata-Ordúz L. Prediction of the flexural capacity of steel fiber reinforced self-compacting concrete beams combining neural networks, the Barcelona test and the gravitational search algorithm. *Res. Eng. Struct. Mater.*, 2025; 11(5): 2437-2466.

Disclaimer

All the opinions and statements expressed in the papers are on the responsibility of author(s) and are not to be regarded as those of the journal of Research on Engineering Structures and Materials (RESM) organization or related parties. The publishers make no warranty, explicit or implied, or make any representation with respect to the contents of any article will be complete or accurate or up to date. The accuracy of any instructions, equations, or other information should be independently verified. The publisher and related parties shall not be liable for any loss, actions, claims, proceedings, demand or costs or damages whatsoever or howsoever caused arising directly or indirectly in connection with use of the information given in the journal or related means.



Published articles are freely available to users under the terms of Creative Commons Attribution - NonCommercial 4.0 International Public License, as currently displayed at here (the "CC BY - NC").



Research on Engineering Structures & Materials



www.jresm.org

Research Article

Prediction of the flexural capacity of steel fiber reinforced self-compacting concrete beams combining neural networks, the Barcelona test and the gravitational search algorithm

David Cotes-Prieto *,a, Luis Zapata-Ordúz b

Grupo de Investigación en Materiales de Construcción y Estructuras (INME), Universidad Industrial de Santander, Escuela de Ingeniería Civil, Colombia

Article Info

Abstract

Article History:

Received 08 Dec 2024 Accepted 24 Jan 2025

Keywords:

Steel fiber reinforced self-compacting concrete;
Barcelona test;
Artificial neural networks;
Gravitational search algorithm;
Non-linear finite element analysis

Steel fiber reinforced self-compacting concrete (SFRSCC) has improved fresh and hardened state properties compared to conventional concrete. Nonetheless, experimentally validated tools to model its flexural capacity are still required to encourage its massive application in civil infrastructure. This research assessed the maximum bending moment (Mu) of SFRSCC beams in four-point loading using an Artificial Neural Network (ANN). The experimental program considered waterbinder ratios (w/b) from 0.40 to 0.60 and steel fiber ratios (%F) from 0.00% to 1.00% in volume. Compressive and tensile behaviors were obtained by combining constitutive models based on uniaxial compression and double-punching Barcelona tests. A modification to the existing Barcelona test constitutive model is proposed to improve post-peak stress prediction. To increase the amount of data needed for proper training of the ANN, non-linear finite element analyses (NLFEAs) were executed through commercial software. NLFEAs were fed using the constitutive relationships from tests. ANN inputs were w/b, and %F, and the output was Mu. Different ANN architectures were evaluated and trained using Momentum Back-Propagation, Particle Swarm Optimization, and Gravitational Search Algorithm (GSA). Results showed that the ANN trained with GSA accurately predicted (R²=0.99) the Mu.

© 2025 MIM Research Group. All rights reserved.

1. Introduction

Nowadays, concrete is the most used structural material in the construction industry (1). Nonetheless, hardened Conventional Concrete (CC) has low tensile strength, ductility, and tenacity (2,3). Therefore, its use in practice requires incorporating reinforcement to improve its mechanical properties, with steel rebar being the most common choice. Additionally, CC has limited workability in fresh state, so low quality control during casting elements with high rebar ratios can lead to discontinuities due to poor consolidation or undesired reinforcement movements, compromising the structural capacity and durability (4,5).

Hence, to overcome these disadvantages, research attention has been addressed on Steel Fiber Reinforced Self-Compacting Concrete (SFRSCC). SFRSCC improves the CC fresh state properties, allowing it to flow through the formwork mainly by its self-weight with low or no need of vibration. Therefore, higher quality elements are achieved due to the more uniform consolidation during pouring (4–6). Moreover, in hardened state, the addition of steel fibers contributes to control cracking as these markedly improve SFRSCC tensile and strain capacity, compared to CC (2,3,7,8). Consequently, the rebar required can be reduced without compromising strength and ductility (7,9). Despite its benefits, manufacturing SFRSCC requires higher amounts of binder than CC. Hence, its cement consumption is reduced by using supplementary cementitious materials, such as

*Corresponding author: dscotpri@correo.uis.edu.co

^aorcid.org/0000-0001-7761-1617; ^borcid.org/0000-0001-8586-602X

DOI: http://dx.doi.org/10.17515/resm2025-569ml1208rs Res. Eng. Struct. Mat. Vol. 11 Iss. 5 (2025) 2437-2466

fly ash, which not only allows SFRSCC to be more cost-effective material but also diminishes its carbon-print (10,11).

The improved characteristics of SFRSCC make it a feasible candidate for wide use in civil infrastructure, which is often subjected to flexure (therefore, tensile stresses and strains). Literature reports show successful implementations of SFRSCC in bending subjected structures, such as buildings, retaining walls, slabs, pipes, and tunnels (3,9,12–15). However, its massive application is scarce in many countries due to the usual need for time and money-consuming laboratory tests to assess its flexural capacity. The main reason behind this is the lack of reliable models and practical tools to predict SFRSCC members hardened state mechanical properties. For instance, in Colombia, the national standard for structural design of buildings (NSR-10) demands intense flexural testing to monitor the cracking strength and post-peak behavior. This standard also lacks on recommendations for theoretically assessing SFRSCC mechanical behavior (16).

Many researchers have published different alternatives to predict the flexural strength of SFRSCC, most based on constitutive modeling of the tensile response along with Non-Linear Finite Element Analysis (NLFEA). Moradi et al. (17) proposed a constitutive model including the post-peak behavior of Steel Fiber Reinforced Concrete (SFRC) based on the results of direct tensile and compressive tests. They successfully implemented the model along with NLFEA to predict the ultimate flexural capacity of beams. Lee et al. (18) modeled the constitutive behavior of SFRC using exponential functions, where the parameters were obtained through bending tests. This model, although functional, still requires the use of expensive laboratory tests. Huo et al. (19) published a stress-strain model that included the orientation effect of the fibers. The inputs of the model were basic material and geometric parameters, easy to obtain with no need for complex testing. The feasibility of the model was proved by accurately predicting the load-displacement curves of beams modeled with NLFEA. Nonetheless, the equations are non-linear and complex, requiring vast knowledge by the practitioner who may use them for applied cases.

An interesting approach to modeling the constitutive behavior of SFRC was presented by Blanco et al. (20). They established simplified equations to assess the tensile behavior of the material based on the results of the Barcelona test. The Barcelona test is a double punching test that captures the tensile response of SFRC with several advantages over the bending and uniaxial tensile tests. It is less time and material-consuming, easier to perform, and its results at different samples of equal dosage exhibit less statistical scatter (20). Nonetheless, the equations underestimated the strength of the material during the post-peak behavior. Moreover, NLFEA may still be required to determine the flexural response of SFRSCC structural elements.

The models previously mentioned may still discourage the implementation of SFRSCC in the industry since they require precise knowledge of constitutive modeling and NLFEA. A more engineering-oriented and user-friendly tool that may be an incentive for the use of SFRSCC is the Artificial Neural Network (ANN). Although training an ANN implies lots of experimental and numerical work, its final usage by a practitioner is straightforward. That is why ANN has been successfully used in civil engineering to predict complex outputs based on simple inputs. Chopra et al. (21) trained an ANN to estimate the compressive strength of concretes varying the curing age and the fly ash content. The investigation yielded R²>0.80, which indicates good prediction capacity. Hodhoh et al. (22) achieved an ANN capable of predicting SFRC strength properties, such as compressive and impact resistance, based on the dosage of the concrete.

The need for tools that reduce the number of experiments required to predict the flexural capacity of SFRSCC concrete beams is imperative to its massive use in industry. Therefore, this investigation assessed an ANN capable of predicting the flexural strength of SFRSCC concrete beams loaded in the Four Points Bending Test (FPBT). The FPBT was here used as pure bending (no shear force) occurs at the midspan between loads, contrary to other flexural tests such as the Three Point Bending Test (23). Hence, the FPBT is a highly suitable test to achieve a more realistic characterization of the bending moment capacity of SFRSCC beams (23–25).

On the other hand, the input variables for the experiments were the simple parameters water/binder ratio (w/b) and the ratio of hooked-end fibers added by volume (%F). The output was the ultimate bending moment (M_u). The training of the ANN was done by several NLFEAs and

validated with real FPBT. The NLFEA models were fed with constitutive relations calibrated with the results of uniaxial compressive and Barcelona tests. Moreover, a modification was implemented to improve the constitutive model for tensile stress-strain based on the Barcelona test proposed by Blanco et al. (20). The original model was reported by their authors to under-estimate the post-peak stresses of the SFRSCC. In that sense, the change here proposed aimed to face this issue by rewriting the equilibrium equations using the free body diagram of the cracked specimen, contrary to the original set-up of equations which was based on the uncracked configuration. The modification was found to more precisely predict the post-cracking behavior of the material.

2. Materials and Methods

This section describes the experimental campaign performed, constitutive modeling, the NLFEA executed, and the training and validation of the ANN.

2.1 Experimental Campaign

Variables considered for the SFRSCC mixtures were %F from 0.00% to 1.00% (0 to 78 kg/m³) and w/b from 0.40 to 0.60. The fibers were hooked-ended and had a tensile strength of 1200 [MPa], length L=60 [mm], diameter d=0.75 [mm], and aspect ratio L/d=80. Ranges of %F and w/b were chosen due to their common use in Colombia according to local providers. The combinations of %F and w/b for the mixtures to test were determined using a Central Composite Design (CCD). A CCD is a type of statistical design of experiments that combines the 2^k factorial design, with $2 \cdot k$ axial points and 1 to 5 central points. The 2^k factorial design is an efficient statistical experimental design that allows to evaluate the simultaneous effect of k factors (in this case %F and w/c) on a response (in this case, the M_u) for a physical phenomenon, by using a minimum number of experimental observations (26). Moreover, the addition of the axial and central points allows fitting the model to a second order response surface. Subsequently, optimization of the factors can be performed (26). Additionally, the use of more than one central point enhances the accuracy of the estimated results on the middle of the experimental domain (26). In addition to the CCD experiments, four control mixtures with no fibers (M 40-00, M 43-00, M 57-00, and M 60-00) were added to evaluate the influences of fibers.

The self-compacting behavior of the mixtures was achieved following the mix design recommendations of Okamura (5), including the use of a super-plasticizer (SP) and a 15% mass replacement of fly ash. The fresh state properties of fluidity and viscosity of the mixtures were considered adequate when the slump-flow test diameter (SFD) was between 520 and 900 [mm], and the T₅₀₀ test time was below 10 [s], according to EFNARC (27). Table 1 shows the mixture proportions and their fresh state control test results. The notation first indicates the w/b ratio and, second the %F. For each mixture, three batches were manufactured to cast all the specimens described ahead. An exception was considered for the central point M 50-50, where five times more batches (15 batches) were casted. This decision was adopted in order to enhance the statistical accuracy of the results according to the literature (26). Therefore, in the subsequential sections, the number of specimens tested for M 50-50 is always five times the other mixtures. Some of the results of this experimental plan have already been published by the authors (28). The concrete was used to cast cylinders for uniaxial compression tests, Barcelona, and beams for FPBT. Due to limited availability of the test equipment at the university where the experimental campaign was developed, all tests had to be performed at an age of 147 days. Although the typical testing age for structural design purposes according to the standards is 28 days for conventional concretes (up to 56 days for concretes including pozzolanic admixtures), the testing at further ages does not constitutes a major problem from the point of view of the authors as typically, more than 90% of the strength has already developed at these design ages (29). Therefore, the strength obtained testing at 147 days will more likely represents a difference (below 10%) respect to the typical design test ages that does not negatively impact the purposes of this study.

Table 1. Mix proportions and fresh state test results

Mix	w/b	%F	Cement	Fly-ash	Coarse	Fine	SP	SFD	T ₅₀₀
			kg/m³	kg/m³	kg/m³	kg/m³	kg/m³	mm	S
M 40-00	0.40	0.00	526.09	78.91	410.91	958.78	3.39	695.00 (62.85)*	3.31 (2.53)*
M 40-50	0.40	0.50	526.09	78.91	406.90	949.42	2.96	716.67 (21.60)*	3.10 (1.11)*
M 43-00	0.43	0.00	506.74	76.01	410.16	960.79	2.80	673.33 (112.37)*	3.27 (3.21)*
M 43-15	0.43	0.15	506.74	76.01	410.52	956.48	2.10	626.67 (45.02)*	2.43 (0.71)*
M 43-85	0.43	0.85	506.74	76.01	404.43	943.66	2.62	576.67 (49.26)*	6.93 (0.98)*
M 50-00	0.50	0.00	459.13	68.87	412.39	958.38	2.01	575.00 (18.71)*	1.12 (0.21)*
M 50-50	0.50	0.50	459.13	68.87	412.39	958.38	2.01	674.93 (68.85)*	1.28 (0.32)*
M 50-100	0.50	1.00	459.13	68.87	407.24	950.22	2.01	705.00 (133.98)*	1.62 (0.97)*
M 57-00	0.57	0.00	411.18	61.68	426.37	994.84	1.23	556.67 (28.75)*	1.00 (0.00)*
M 57-15	0.57	0.15	411.18	61.68	425.20	992.10	1.23	645.00 (12.25)*	1.00 (0.00)*
M 57-85	0.57	0.85	411.18	61.68	418.45	979.97	1.37	621.67 (123.84)*	2.10 (0.97)*
M 60-00	0.60	0.00	400.00	60.00	424.71	990.99	0.78	556.67 (29.44)*	1.00 (0.00)*
M 60-50	0.60	0.50	400.00	60.00	421.62	980.68	1.29	701.67 (39.71)*	1.00 (0.00)*

^{*}Average (Standard deviation)

2.2 Testing and Methods of Processing Results

2.2.1 Uniaxial Compression Tests

For each mixture, four cylinders of 75x150 [mm] were tested in monotonic load according to ASTM C39 (30). The deformation rate was 1.50 [mm/min] up to an actuator displacement of 6 [mm]. Compressive strength was calculated from the experimental results. Examples of the tested cylinders are presented in Figure 1 and average results of the compressive strength, $f_{c\ avg}$, are presented in Figure 2. A detailed statistical analysis of the compressive strength is presented in the results section.

2.2.2 Barcelona Tests

Double punching Barcelona Tests were performed in 4 cylinders of 150x150 [mm] for each mixture. The punching effect was achieved by placing two cylindrical steel punches of diameter 37.5 [mm]. The test was performed according to the standard UNE-83515 (31). The deformation rate was monotonic at 0.50 [mm/min] up to an actuator displacement of 6 [mm].

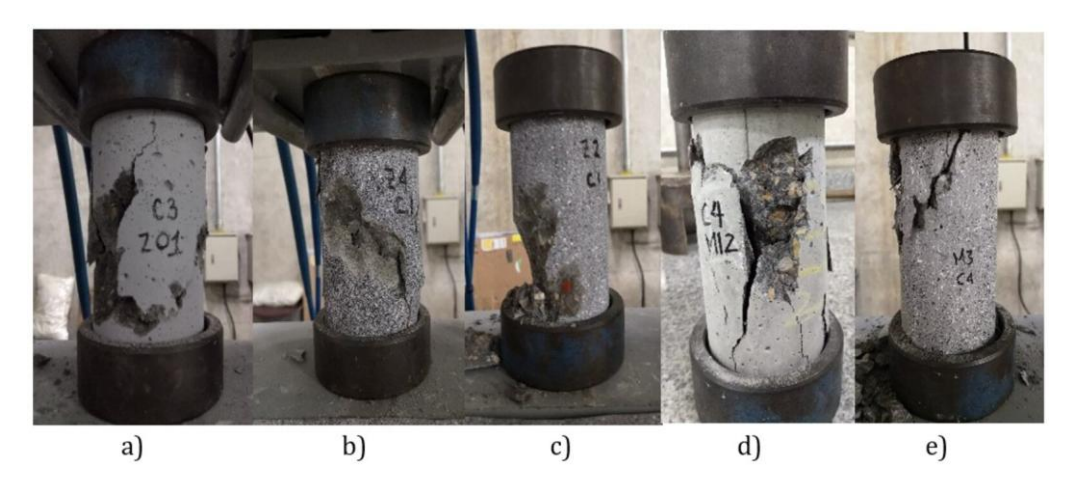


Fig. 1. Compressive strength tested cylinders: a) M 40-00, b) M 60-00, c) M 43-00, d) M 43-10 and e) M 43-85.-

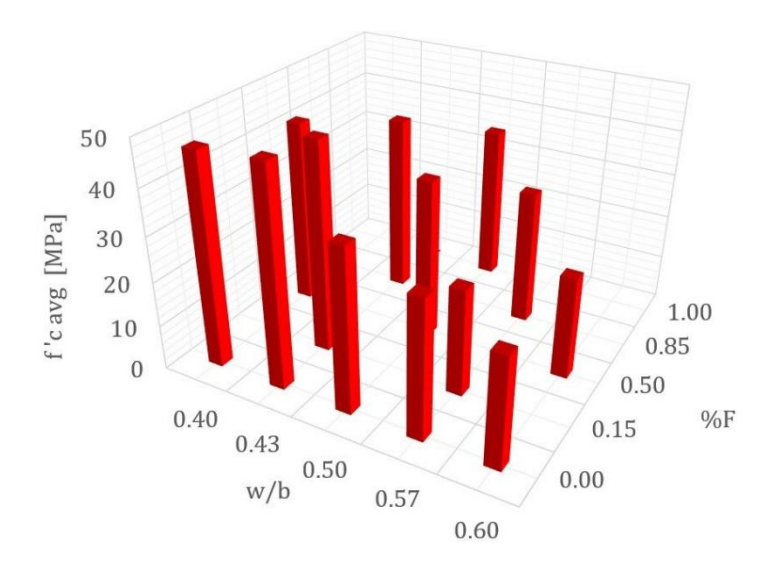


Fig. 2. Average compressive strength as function of w/b and %F

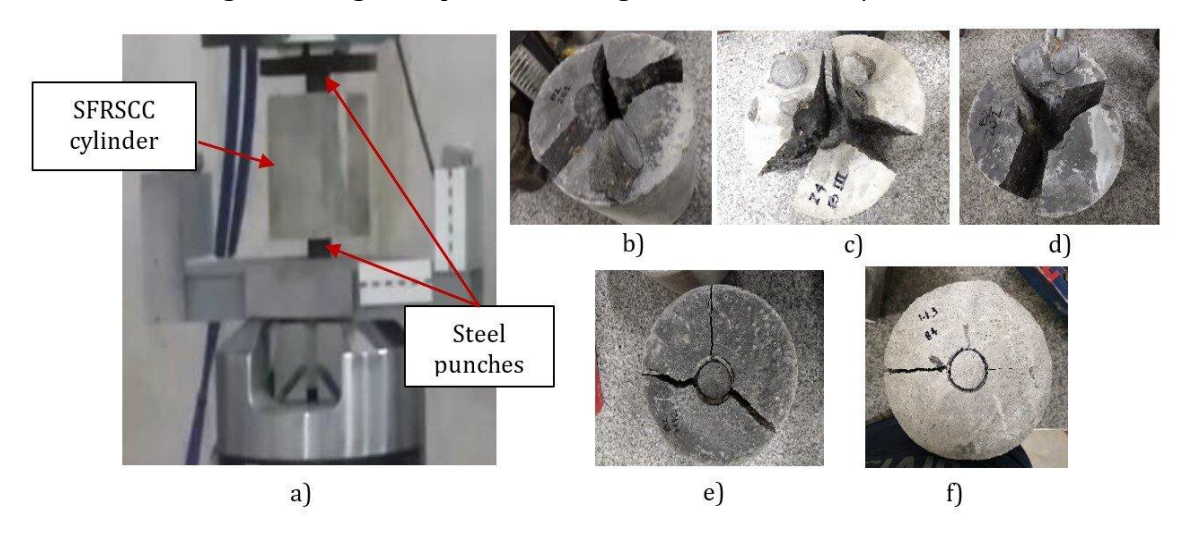


Fig. 3. Barcelona test cylinder: a) Set-up, b) M 40-00, c) M 60-00, d) M 43-00, e) M 43-10 and f) M 43-85

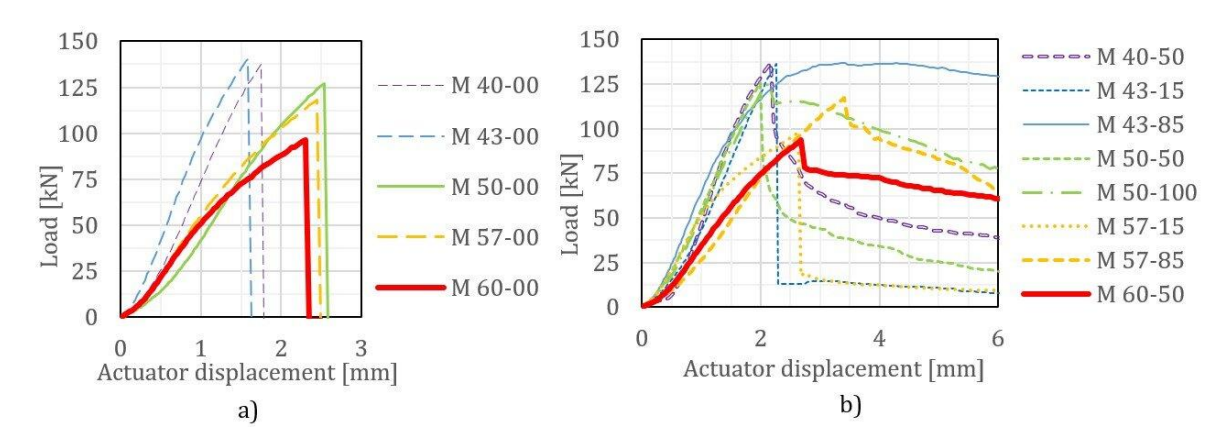


Fig. 4. Load-displacement curves for Barcelona cylinders: a) without fibers, and b) with fibers.

For reference, Figure 3 shows the test set-up and various tested cylinders. Also, examples of the load-actuator displacement curves experimentally obtained are showed in Figure 4. The data from these curves was used as the main input to determine the tensile stress-strain curve of the specimens as described in Section 2.2.6.

2.2.3 Four Points Bending Tests

The FPBTs were performed in four beams of 150x150x500 [mm] for each mixture, following the standards ASTM C1609 and RILEM TC 162-TDF (32,33). Since pure bending occurs at the central length, a notch of depth 22 [mm] and thickness 0.4 [mm] was cropped in the mid-span of the specimens to arouse the cracking there. The free length between supports at testing was 450 [mm], and the separation between loaded points 150 [mm]. Set-up of the test and some examples of beams at the end of the test are shown in Figure 5. Also, examples of the load-actuator displacement curves are presented for every mixture in Figure 6.

During the test, the deformation rate was incremental and varied depending on the actuator displacement: 0.20 [mm/min] from 0 to 1 [mm], 0.25 [mm/min] from 1 to 5 [mm], and 0.70 [mm/min] from 5 to 10 [mm]. As Bernard [29] described, the actuator displacement is not representative of the deflection (flexural deformation) the beam experiences. Therefore, Digital Image Correlation (DIC) was used to measure the mid-span deflection on the beams at each load increment. Details on this procedure can be found in a previous publication by the authors (28). The bending moment at each load was calculated using the equilibrium equations. Finally, the experimental moment-deflection curves were obtained for each tested beam.

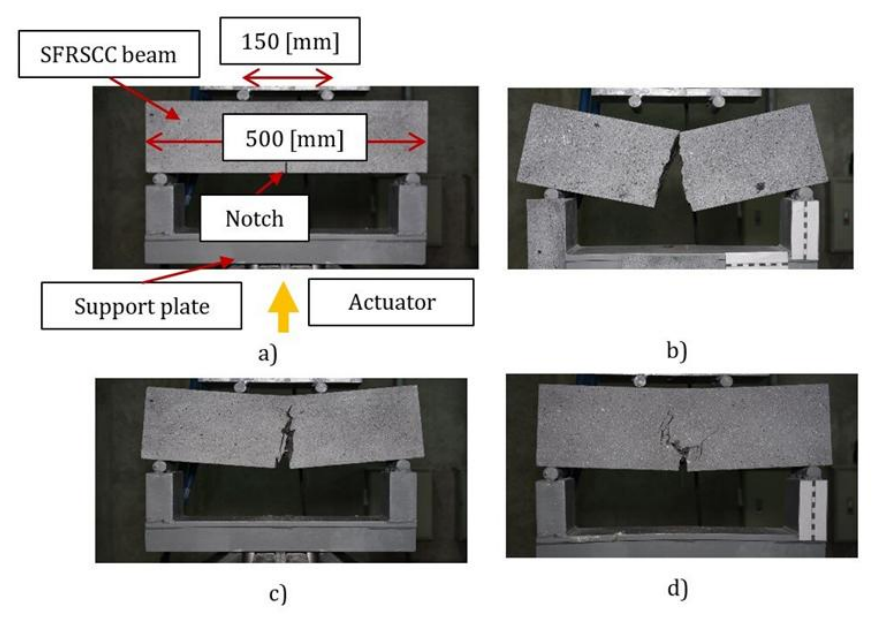


Fig. 5. FPBT beams a) Set-up, b) M 50-00, c) M 50-50, and d) M 50-100

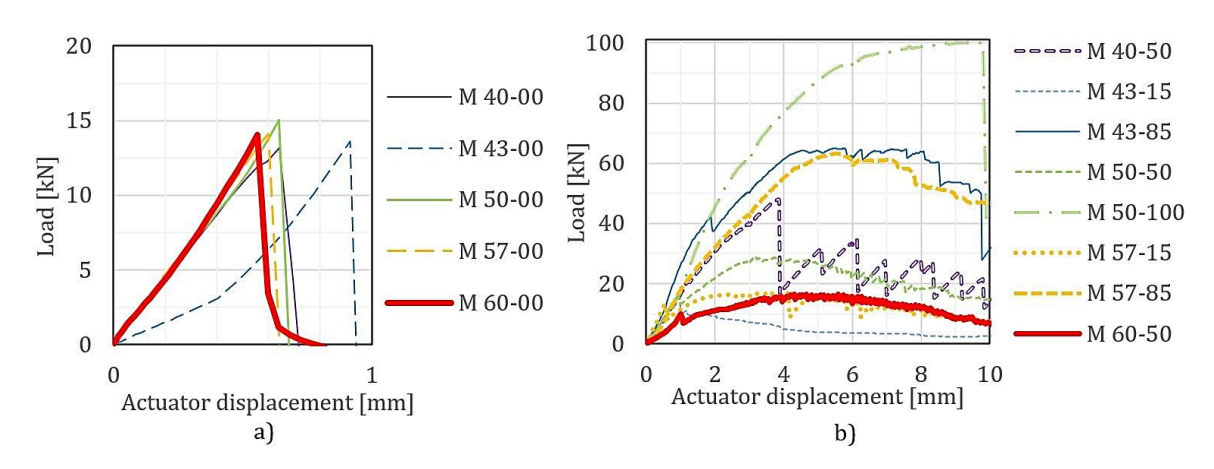


Fig. 6. Load-displacement curves for FPBTs beams: a) without fibers and, b) with fibers

2.2.4 General Aspects on The Implemented Constitutive Models

The constitutive models for the compressive and tensile stress-strain responses of the mixtures were selected based on the literature review. The compression behavior was based on the

equations proposed by Wang et at. (34) and De Oliveira (35). The tensile response was based on the model proposed by Blanco et al. (20), Bortolotti (36) and modifications to these proposed by the authors of this paper.

In all cases, the material was considered homogeneous and isotropic. The shear response was assumed to be linear, and the Poisson ratio was fixed as 0.20. This analysis was performed only for the nine mixtures part of the CCD (M 40-50, M 43-15, M43-85, M 50-00, M 50-50, M 50-100, M 57-15, M 57-86 and M 60-50 in Table 1).

2.2.5 Compressive Stress-Strain Constitutive Relation

The non-linear model implemented here was described by Wang et al. (34) and is presented equation (1). It includes the effect of fibers on compressive strength.

$$f_{c} = \begin{cases} f_{c}' \frac{\epsilon_{c}}{\epsilon_{c}'} \left(\alpha_{a} + (3 - 2\alpha_{a}) \frac{\epsilon_{c}}{\epsilon_{c}'} + (\alpha_{a} - 2) \left(\frac{\epsilon_{c}}{\epsilon_{c}'} \right)^{2} \right) & \epsilon_{c} < \epsilon_{c}' \\ f_{c}' \frac{\epsilon_{c}}{\epsilon_{c}'} \left(\frac{1}{\alpha_{d} \left(\frac{\epsilon_{c}}{\epsilon_{c}'} - 1 \right)^{2} + \frac{\epsilon_{c}}{\epsilon_{c}'} \right) & \epsilon_{c} \ge \epsilon_{c}' \end{cases}$$

$$(1)$$

In these equations f_c is the compressive stress in [MPa] evaluated at an axial strain ϵ_c in [mm/mm], and f'_c and ϵ'_c are the compressive strength in [MPa] and its associated axial strain in [mm/mm], respectively. The shape factors α_a and α_d were calculated using the linear relations of equations (2) and (3). These equations were obtained using the empirical values of α_a and α_d published by Wang et al. (34) for %F (by volume) of 0.00 and 1.00.

$$\alpha_a = 1.5 + 0.2(\%F) \tag{2}$$

$$\alpha_d = 5.4 - 3.9(\%F) \tag{3}$$

The value of f_c' was obtained from the compressive uniaxial tests with the peak load and the cross-sectional area of the cylinder. Since the actuator displacement was not a trustable measure of the axial deformation, ϵ_c' was not determined experimentally. Equation (4), as reported by De Oliveira et al. [31], was used. It was chosen as the materials, types of fibers, and %F used in their investigation were similar to those used in this work.

$$\epsilon_c' = (0.00048 + 0.0001886(\%F)) \ln(f_c')$$
 (4)

2.2.6 Tensile Stress-Strain Constitutive Relation

The model used was based on the proposal of Blanco et al. (20). It was chosen as it directly relates the tensile stress and strain of the SFRSCC to the load-actuator displacement curve obtained from the Barcelona test. The model assumes the material follows a linear stress-strain relation up to the peak cracking stress f_r , then captures the residual stresses and their related strain after cracking. This residual behavior is the main contribution of the steel fibers. Blanco et al. (20) reported that their original model underestimates the cracking peak and residual stresses compared to other models validated by international standards. Therefore, two modifications on the calculus of the stresses were proposed here to improve the model:

• The value of f_r in [MPa] was calculated using equation (5) proposed by Bortolotti (36), which is based on the Mohr-Coulomb failure criteria applied to concrete cylinders in double punching.

$$f_r = \frac{P_r}{\pi \left(\frac{dh}{2} - \frac{d_c^2}{4\tan(\theta)}\right)} \tag{5}$$

Here, d and h are the diameter and height in [mm] of the SFRSCC cylinder, P_r is the peak load (cylinder cracking load) obtained from the Barcelona test in [N] and d_c and β are the base in [mm]

and inclination angle in [°], of the conical wedge formed by the cylinder cracking, as shown in Figure 7.

The values of P_r and d_c were measured for each cylinder after performing the tests. However, β was not calculable for all tests as the wedge was still harshly attached by the fibers to the fractured specimen. In the cases where β was measured, it was close to 25°, which agrees with the value reported by (20). Therefore, this value was used in the equation.

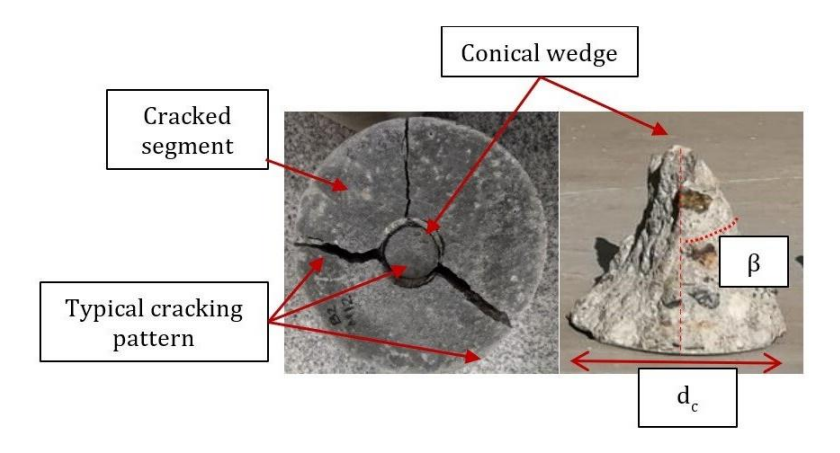


Fig. 7. Typical fracture of a cylinder on Barcelona test

• The equilibrium equations that related the load to the tensile stress in the post-cracking stage were rewritten on a cracked segment of the cylinder (cracked configuration) instead of on a differential element (reference configuration) as initially proposed by Blanco et al. In the opinion of the authors, this approach is more consistent with the actual phenomenon since the cracking of the cylinder is discrete instead of smeared. Therefore, the action of fibers and residual tensile stresses occurs at the cracked surfaces.

For the equilibrium, the same forces considered by Blanco et al. were included, and it was assumed that the cylinder fractured into equal pieces. Figure 8 illustrates the cracked segment for the equilibrium.

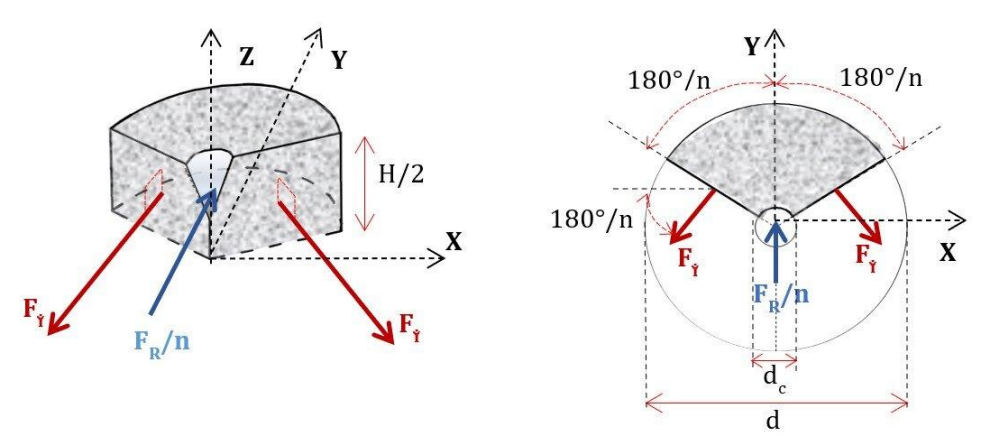


Fig. 8. Free body diagram of the cracked cylinder segment for equilibrium

In this figure, n is the number of cracked segments of the cylinder, which may be different for each test but is usually 2, 3 or 4. F_i are the forces in [N] that act on the XY plane, orthogonal to the cracked surfaces and hold together the segments of the cylinder, mainly due to the action of fibers. F_R is the force in the plane XY resulting from the contact between the wedge and the cracked segment, which is calculated according to (20) using the equation (6).

$$F_R = P\left(\frac{\cos(\beta) - \mu_k \sin(\beta)}{\sin(\beta) + \mu_k \cos(\beta)}\right) \tag{6}$$

In this equation, P is the actuator load in [N] and μ_k is the kinetic friction coefficient between wedge and segment. Specifically, μ_k represents the ratio between the friction (tangential) and contact (normal) forces that generates in the contact between the conical wedge and the cracked segments of the cylinder during the Barcelona test (see Figure 7). A detailed description of these forces can be found in (20). According to the literature, common assumed values of μ_k used between 0.5 and 1.4 (20,37). In this research, in order to make a more precise estimation of μ_k , its calculation was done using inverse analysis aiming to lower the error between the modeled tensile behavior of the SFRSCC and the actual experimental results. Performing force equilibrium along Y in Figure 8 yields equation (7).

$$-2 F_i \sin\left(\frac{180^\circ}{n}\right) + \frac{F_R}{n} = 0 \tag{7}$$

Then, the tensile stress f_t is calculated by replacing (7) and (6), solving F_i and dividing it by the cracking surface. Equation (8) shows this solution.

$$f_t = \frac{P\left(\frac{\cos(\beta) - \mu_k \sin(\beta)}{\sin(\beta) + \mu_k \cos(\beta)}\right)}{2 n \sin\left(\frac{180^\circ}{n}\right) \left(\frac{d h}{4} - \frac{d_c^2}{8 \tan(\beta)}\right)}$$
(8)

Notice that the only difference between this equation and the original proposal of Blanco et al. is the expression $n \sin\left(\frac{180^{\circ}}{n}\right)$, which corresponds to π in the original equation. If $n \to \infty$ then $n \sin\left(\frac{180^{\circ}}{n}\right) \to \pi$, which is the equilibrium on a differential. For n between 2 and 4, this denominator is always lower than π , which results in higher residual stresses, therefore, a more accurate estimation in comparison to the original model.

Strains were calculated following the kinematic equations (9) deduced by Blanco et al. (20). Furthermore, it is worth mentioning that for the post-cracking stage, their equations considered the cracked configuration of the cylinder. Therefore, the proposed approach for deducing the equilibrium equations from the cracked segments is consistent with these original kinematic equations.

$$\epsilon_{t} = \begin{cases} \frac{f_{r}}{E_{c}} & \text{at cracking} \\ \frac{n U_{z}}{\pi \left(\frac{d}{2}\right)} \tan(\beta) \sin\left(\frac{180^{\circ}}{n}\right) & \text{post-cracking} \end{cases}$$
(9)

Here, ϵ_t is the tensile strain in [mm/mm], U_z is the actuator displacement in [mm], d is the cylinder diameter in [mm], f_r the peak cracking stress in [MPa] and E_c is the elastic modulus of the SFRSCC in [MPa]. The last was assumed as the initial tangent modulus obtained by differentiating the equation (1) according to reference (19).

Equations (5), (8) and (9) were used to determine the tensile stress-strain curve of the SFRSCC. Due to the vast amount of data collected during the Barcelona test, Blanco et al. [20] recommended simplifying the model to a quadrilinear model. Nevertheless, here it was necessary to use a pentalinear model to achieve convergence of the NLFEA, which was further described. The strain points in [mm/mm] considered for the pentalinear stress-strain curve were: (i) $\frac{f_r}{E_c}$, (ii) $\frac{f_r}{E_c}$ + 0.0005, (iii) $\epsilon_t = 0.0005$, (iv) $\epsilon_t = 0.0075$ and (v) $\epsilon_t = 0.015$. For these strains the related stresses were calculated. These were respectively noted as f_{t1} , f_{t2} , f_{t3} , f_{t4} and f_{t5} .

2.2.7 Characteristic stress-strain curves

For all the mixtures, four specimens in compression and four in Barcelona double punching were tested. Each specimen had different stress-strain curves, which is expected since there is statistical scatter due to factors such as inherent concrete heterogeneity. Hence, characteristic stress-strain

curves for each mixture were determined by fitting the sample results to the Weibull two-parameter distribution, selected as it has been proven to be adequate to model the statistical variation of ceramic materials such as concrete (38,39). Weibull formula is presented in equation 10, where f_W is the probability density, x is the studied variable, β_W is the scale parameter (similar to mean in normal distribution), λ_W is the shape parameter (similar to standard deviation in normal distributions).

$$f_W = \frac{\lambda_W}{\beta_W} \left(\frac{x}{\beta_W}\right)^{\lambda_W - 1} e^{-\left(\frac{x}{\beta_W}\right)^{\lambda_W}} \tag{10}$$

The Weibull parameters for each mixture (Table 1) were calculated for f_c' , f_{t1} , f_{t2} , f_{t3} , f_{t4} and f_{t5} and f_{t5} , using the Maximum Likelihood Method (MLM) through MATLAB R 2020a (40). MLM was implemented as it is a widely used optimization technique which aims to determine the parameters of a probability density function that the maximizes the likelihood that the experimental results belong to the Weibull distribution (38). After fitting the parameters, the goodness of fit of the results was evaluated using the Anderson-Darling test (AD2). The MATLAB script used to calibrate the Weibull parameters and determine the AD2 is presented in the Appendix 1.

2.2.8 Non-Linear Finite Element Analysis

NLFEAs were performed using SAP2000® V.22 (41) to determine the flexural response of beams on FPBT for each mixture. The finite element used was a four-nodes membrane and the material non-linearity was incorporated using multi-linear stress-strain relations based on the characteristic constitutive models calculated as explained in Section 2.2.3. The mesh showed in Figure 9 was determined using convergence analysis, in which a relative error of 0.05% in the peakload was achieved using 960 elements.

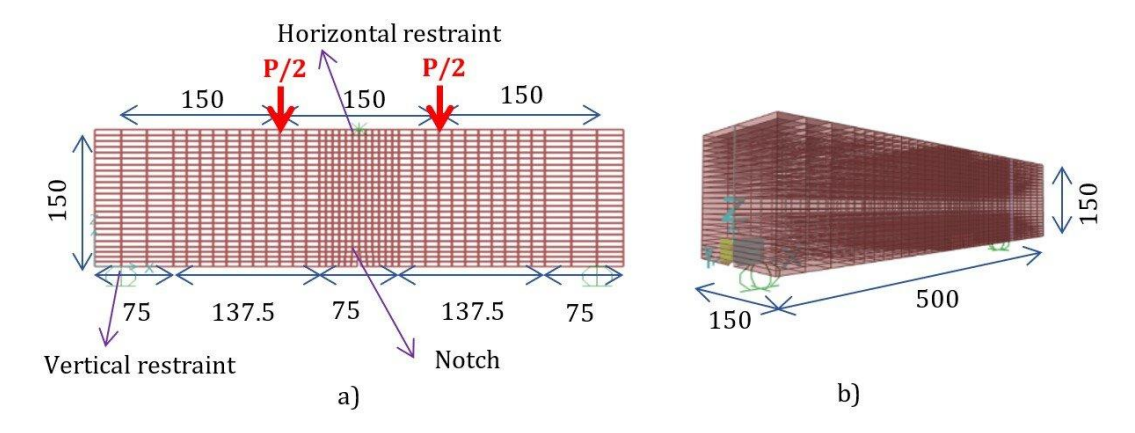


Fig. 9. Finite elements model, a) Front view, b) Extruded view. All distances in [mm]

The analyses were displacement-controlled with 500 steps, up to an objective displacement of 0.25 [mm] at mid-span. SAP2000® uses Newton methods to solve the equilibrium at each step (42). All the analyses were performed on a laptop ASUS N550J with Intel® CoreTMi7 processor, four cores, and 16 [GB] of RAM. The time of the analyses was between 5 and 30 minutes. The parameter μ_k was used to calibrate the NLFEA to the FPBT experimental results by using inverse analysis. This analysis was performed iteratively varying the values of μ_k in the constitutive tensile models, then calculating the numerical maximum bending moment and comparing it to its experimental value. The procedure was continued until the theoretical value was close to the experimental. Obtained μ_k values were between 0.5 and 1.4 as expected, according to (20). The load-deflection curve was obtained from each simulation, and then M_u was determined from equilibrium using the peak load.

2.2.9 Data Set for The Artificial Neural Network

Proper training, calibration, and validation of ANNs, requires several data sets (43). The experimental program only provided 13 data with inputs w/b and %F, and output M_u , therefore, NLFEA was used to increase the amount of data. This required determining the constitutive model

parameters for different w/b and %F among the studied ranges. Hence, a Response Surface (RS) based on the 2^k with central and axial points experimental designed used (see Section 2.1), was calculated for each one of the characteristic values f_c' , f_{t1} , f_{t2} , f_{t3} , f_{t4} , and f_{t5} . Equations (11) to (16) are the RSs between the constitutive model parameters in [MPa] and the inputs w/b and %F obtained with Minitab V.16® (44). Moreover, for all these equations R²>0.89, which indicates good fitness to the experimental data.

$$f_c' = -459.40 \left(\frac{w}{b}\right)^2 + 118.80 \left(\%F\right) \left(\frac{w}{b}\right) - 59.30 \left(\%F\right) + 291.20 \left(\frac{w}{b}\right) + 7.20 \tag{11}$$

$$f_{t1} = -0.74 \, (\%F)^2 - 40.16 \, \left(\frac{w}{b}\right)^2 + 11.17 \, (\%F) \, \left(\frac{w}{b}\right) - 4.80 \, (\%F) + 29.59 \, \left(\frac{w}{b}\right) - 1.44$$
(12)

$$f_{t2} = -3.19(\%F)^2 - 59.10\left(\frac{w}{b}\right)^2 + 6.15(\%F)\left(\frac{w}{b}\right) + 55.10\left(\frac{w}{b}\right) - 12.65$$
 (13)

$$f_{t3} = 0.13(\%F) + 2.98 \tag{14}$$

$$f_{t4} = 1.12 \, (\%F)^2 + 1.37 \, (\%F) - 2.09 \, \left(\frac{w}{b}\right) + 1.10$$
 (15)

$$f_{t5} = 1.73 \, (\%F)^2 + 0.35 \, (\%F) - 2.38 \left(\frac{w}{b}\right) + 1.27$$
 (16)

These equations were evaluated for w/b from 0.40 to 0.6 in steps of 0.02, and %F from 0.00 to 1.00 in steps of 0.10. Then, the constitutive models were used to determine M_u through NLFEA, as described in Section 2.3. A total of 121 simulations were performed, and their results were consequently used to feed the ANN. The process was automatized through a script that allowed to run SAP2000® using MATLAB®, which is presented in Appendix 2.

2.2.10 Artificial Neural Network

The ANN was a multilayered perceptron fully connected with supervised learning. The inputs were w/b and %F, and the output was the M_u . All its coding was self-made in MATLAB®. A sketch of the architecture of the ANN is presented in Figure 10.

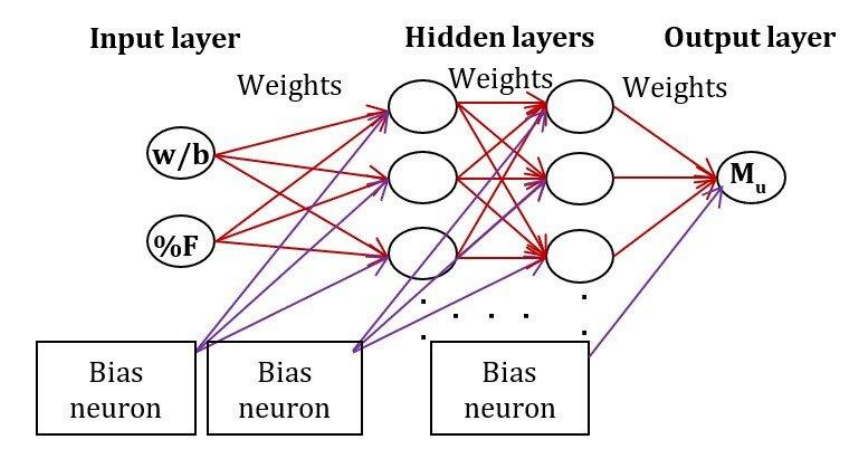


Fig. 10. Architecture of the ANNs

Architectures tested consisted of 1 or 2 Hidden Layers (HL), with 2, 5, 10 or 20 Neurons per Hidden Layer (NHL). For the hidden neurons, the activation function was the hyperbolic tangent, which led to the best results in the preliminary simulations. Moreover, all the input and output data were normalized for the training of the ANN using equation (17), where D_n is the normalized data, D the

original data, and D_{min} and D_{max} the minimum and maximum values of the data before normalization.

$$D_n = \frac{D - D_{min}}{D_{max} - D_{min}} \tag{17}$$

For the assessment of the ANNs, the 121 data were organized in a random permutation according to Ref. (45), then 84 data (\approx 70%) were used for training, 24 (\approx 20%) for calibration, and 13 (\approx 10%) for validation. This division of the data set seeks to avoid the overfitting of the ANN during its training, as described in Ref. (46). The training implied determining the weights (including the bias neurons) to minimize the objective function Mean Squared Error (MSE) presented in equation (18).

$$MSE = \sum_{1}^{N_T} \frac{1}{N_T} (m_{uANN} - m_{uFEM})^2$$
 (18)

Where m_{uANN} are the ultimate moments, normalized according to equation (17), predicted by the ANN, m_{uFEM} are the normalized ultimate moments obtained from the NLFEA of Section 2.2.8, and N_T is the number of training data.

Three optimization methods were evaluated for minimizing the MSE: Momentum Back Propagation (MBP), Particle Swarm Optimization (PSO), and Gravitational Search Algorithm (GSA). The calculation of weights for each architecture was performed five times using each algorithm. MBP and PSO are widely used methods that have proven to be successful in similar ANNs training (45,47,48). A detailed description of these algorithms can be found in (46) and (49). Furthermore, GSA is a meta-heuristic optimization method based on the universal gravity law, developed by Rashedi et al. (50) in 2009, which has been reported to achieve superior performance compared to other algorithms of its class, such as PSO or Genetic Algorithms. Moreover, it has proved to be a feasible alternative to solve optimization problems in structural engineering (51). To the best knowledge of the authors, GSA has not been used for ANNs related to SFRSCC. Therefore, its feasibility was explored here.

In the original nomenclature of the GSA, each iteration is referred to as an age. Its parameters are the initial gravitational constant G_o , the maximum of iterations age_{max} , the shape factor α , the initial number of agents (candidate solutions) N_{oa} , and the relative error tolerance between iterations e_{min} . GSA pseudo-code is as follows:

- Select G_o , age_{max} , α , N_{oa} and e_{min} .
- Make age=1
- Select random values for the N_{oa} agents. In this case each agent is a vector that contains values for the ANN weights (w_i) . This is referred as the position vector of the agent.
- Select random values for the initial velocities of the agents. In this case that refers to the velocity of the weights (Δw_i) .
- Evaluate the objective function for each of the agents. In this case that is the MSE.
- Determine the best and worst agents. Here they are the agents with the lower and higher MSE, respectively.
- Determine the mass of each agent M_a using equation (19).

$$M_a = \frac{MSE - MSE_{max}}{MSE_{min} - MSE_{max}} \tag{19}$$

• Calculate the number of effective agents N_a using equation (20). Effective agents refer to the agents with better values for the objective function MSE. Only these will continue in the next ages.

$$N_a = N_{oa} - \frac{N_{oa}}{age_{max}} age \tag{20}$$

• Calculate the gravitational constant *G* using equation (21).

$$G = G_0 exp^{\alpha \frac{age}{age_{max}}} \tag{21}$$

• Determine the acceleration a_i that acts on each agent. For each (*i*)-th agent, the acceleration that results from its interaction with all the other (*j*)-th agents is calculated using equation (22), where $R_{(i)(j)}$ is the Euclidean distance between the position of agents, ε is a small value to avoid indeterminacy in case both agents have the same position and rand is a random number between 0 and 1.

$$a_{i} = \frac{1}{M_{a(i)}} \sum_{(j)=1,(j)\neq 1}^{N} \left[rand \ G \frac{M_{a(i)} M_{a(j)}}{R_{(i)(j)} + \varepsilon} (w_{i} - w_{j}) \right])$$
(22)

• Recalculate Δw_i using equation (23).

$$\Delta w_{i\,(age+1)} = rand \, \Delta w_{i\,(age)} + a_{i\,(age)} \tag{23}$$

• Recalculate the position of the agents using equation (24). These are the actualized values of the candidate solutions.

$$w_{i\,(age+1)} = w_{i\,(age)} + \Delta w_{i\,(age+1)} \tag{24}$$

- Recalculate MSE for the new position of the agents.
- Actualize the best agent.
- Calculate the relative error between the actualized best agent and the previous best agent.
- Make age=age+1
- If the relative error $< e_{min}$ and age $< age_{max}$, repeat steps VI to XVI.

Different values for the parameters of GSA were tested. The results reported utilized $G_o = 1$, $age_{max} = 1000$, $\alpha = 1$, N_{oa} and $e_{min} = 10^{-15}$, which yielded the lowest values of MSE.

3. Results and Discussion

This section presents the detailed results of the experimental compression, Barcelona and Four Point Bending tests. Also, the results of the constitutive modeling, NLFEA calibration and ANN training are presented and discussed.

3.1. Uniaxial Compression and Barcelona Tests

Table 2 presents the average results of the tests for the compressive and Barcelona tests. In the case of the Barcelona test the table includes the cracking peak load and the tenacity (area under the load-actuator displacement curve), which measures the energy dissipation capacity of the SFRSCC in tension.

Table 2. Compression and Barcelona test results

Mix	Compressive strength	Peak load Barcelona	Tenacity Barcelona
	MPa	kN	J
M 40-00	47.31 (0.06)*	130.09 (0.07)*	111.01 (0.12)*
M 40-50	41.90 (0.03)*	132.69 (0.09)*	370.65 (0.08)*
M 43-00	48.53 (0.03)*	149.64 (0.06)*	134.22 (0.17)*
M 43-15	46.99 (0.04)*	135.29 (0.05)*	202.19 (0.16)*
M 43-85	39.99 (0.11)*	115.52 (0.14)*	426.99 (0.12)*
M 50-00	36.37 (0.04)*	119.56 (0.08)*	132.52 (0.17)*
M 50-50	35.81 (0.11)*	123.98 (0.06)*	332.07 (0.09)*
M 50-100	35.10 (0.15)*	117.15 (0.15)*	504.07 (0.23)*
M 57-00	30.82 (0.09)*	112.28 (0.10)*	139.40 (0.18)*
M 57-15	23.96 (0.03)*	91.87 (0.05)*	167.33 (0.10)*
M 57-85	30.17 (0.01)*	119.85 (0.07)*	508.93 (0.31)*
M 60-00	24.67 (0.02)*	96.54 (0.04)*	128.19 (0.12)*

M 60-50 22.87 (0.10)* 91.42 (0.02)* 323.79 (0.17)*

Average (Coefficient of variation)*

As it is expected for concretes, compressive strength decreases as w/b increases. However, it should be noted that for most of the w/b, the inclusion of fibers reduces the compressive strength between 2% and 18%. This percental decrease is higher for lower values of w/b and increases for higher values of w/b. The same phenomenon has been reported by other researchers (11,52,53) up to decrease values of 25%. The compressive strength decrease might be related to the lost workability of SFRSCC for small values of w/b and high values of w/b, which causes the formation of small voids in the cross sections of specimens during casting. Also, the inclusion of long fibers may generate additional interfacial transition zones by disruption of the binder paste. Both defects promote porous weak zones in the concrete matrix which might increase internal stress concentration during compressive loading, leading to lower compressive capacity.

The peak load Barcelona is a measure of the tensile strength, and it also increases for lower w/b, which is expected for concretes (10). Moreover, the inclusion of fibers had a minor effect on the peak load for most of the mixtures, which is well-known as the main contribution of fibers occurs in the post-cracking stage (54). This effect is evidenced in rises of tenacity between 20% and 280% as the %F augments. This improvement is related to an increase in ductility since tensile strength is marginally affected. Also, Figure 11 evidences the post-cracking contribution of fibers as the cracking width is markedly reduced for higher %F.

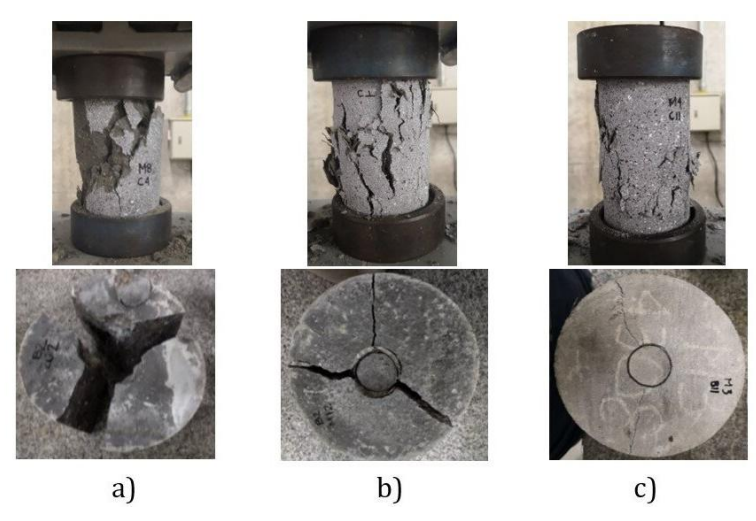


Fig. 11. Compressive and Barcelona test fracture at 6 [mm] actuator displacement for a) M 50-00, M 43-00, b) M 50-50, M 43-15, and c) M 50-100, M 43-85

Coefficients of variation of compressive strength and peak load Barcelona are sharply lower than those of the tenacity. This is evidence of the high statistical scatter existent in SFRSCC mechanical properties that are highly dependent on the fibers. Hence, the use of statistical analysis, as proposed in Section 2.2.3 to characterize the constitutive behavior of SFRSS is imperative. According to the guide ACI-214 (55), coefficients of variation over 0.05 indicate poor agreement of the normal distribution parameters (mean and standard deviation) to the experimental results. Most of these coefficients were higher than this limit, particularly on the tenacity, which is why the Weibull distribution was used to determine the characteristic stress-strain curves, as stated in Section 2.2.3.

3.2 Characteristic Compression Stress-Strain Curves

Fitness of data to the Weibull and Normal distributions to determine the characteristic f_c' are presented in Table 3. P-values of AD² considered as null hypothesis that data belong to the distribution. For a significance level of 0.10, it can be seen that all data fit the Weibull distribution, while M 43-15 and M 60-50 do not adjust to the normal distribution. Moreover, characteristic compressive strength obtained from Weibull analysis was in average 3% higher than those of the normal distribution (mean). Similar results have been published in literature and indicate that the mean is still a good indicator of the characteristic f_c' (56).

Using the Weibull f_c' and the equations of Section 2.2.1, stress-strain curves in compression, were determined and presented in Figure 12. The negative sign indicates compression stress and shrinking strain. From these curves it is seen that SFRSCC initial stiffness E_c is inversely related to w/b. Also, the improvement of residual capacity (post-peak) on higher %F mixes can be noticed as the post-peak stresses on mixes with lower %F (dashed lines) decrease with a steeper slope than those with higher %F (solid lines). This behavior explains the control on compressive cracking perceived in Figure 11 for mixes M 43-85 and M 50-100.

Table 3. Goodness of fit analysis for f'	Table 3.	Goodness	of fit anal	vsis for	f'_c
--	----------	----------	-------------	----------	--------

	W	<i>V</i> eibull	N	ormal
Mix	f' _c	P-value	f'c	P-value
	MPa		МРа	
M 40-50	42.46	0.78	41.90	0.27
M 43-15	47.76	0.74	46.99	0.10
M 43-85	41.88	0.77	39.99	0.24
M 50-00	36.89	0.79	36.37	0.14
M 50-50	38.30	0.52	35.81	0.54
M 50-100	37.07	0.98	35.10	0.77
M 57-15	24.24	0.86	23.96	0.36
M 57-85	30.28	0.89	30.17	0.21
M 60-50	23.70	0.38	22.87	0.01

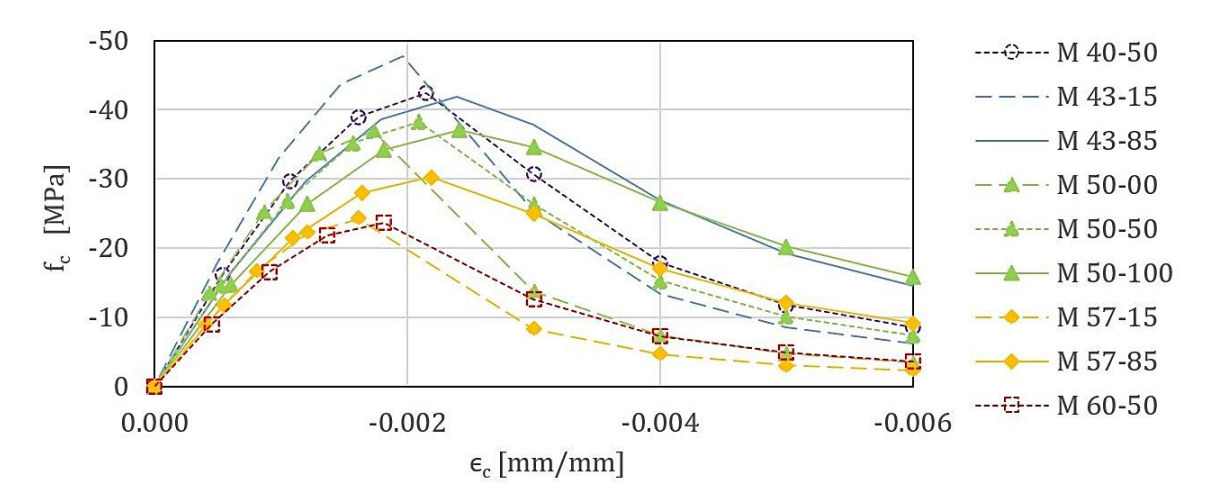


Fig. 12. Compression stress-strain curves

3.3 Characteristic Tensile Stress-Strain Curves

Table 4 presents the five stress parameters for the pentalinear models fitted to Weibull and the μ_k calibrated based on the NLFEA. In this table, the values marked with * did not fulfill the AD² null hypothesis for a significance level of 0.10. These results belong to the M 50-50 for which more experiments were performed, as mentioned in the methodology. Hence, a possible cause of the lack of fitness to Weibull is the blocking effect that might arises from the fact that all the different samples had to be distributed in two different curing chambers with different humidity and temperatures, which could have slightly influenced their strength development (26). Another possible cause of the lack of fitness to Weibull in this case lays in the fact that as it corresponds to the central point, more samples were tested. Hence, according to the statistical theory of the central limit, higher number of samples approximates the observations statistical distribution to a normal distribution (26).

Figure 13 shows the constitutive models calculated using equations of Section 2.2.2. The cracking tensile stresses were, on average, 9.3% of the compressive strength, which is expected for SFRSCC, according to the literature (37). Residual strength (post-peak) increases for higher %F (solid lines)

due to the more bridging action between cracked segments of the concrete, which will occur for more fiber contents.

Nonetheless, the last post-peak slopes (f_{t4} to f_{t5}) were found to be steeper than those reported by other researchers for stress-strain curves obtained with flexure or direct tensile tests (17,35,57). Therefore, underestimation of the stresses at high strain levels occurs. Although conservative for design purposes, a precise prediction of the mechanical behavior requires more work on the constitutive equations. A possible future modification will be to consider that the area where stress is distributed decreases as the segments separate during the Barcelona test.

Mix	f _{t1}	f _{t2}	f _{t3}	f_{t4}	f _{t5}	μ_k
IVIIX	MPa	MPa	MPa	MPa	MPa	
M 40-50	3.61	2.58	2.31	1.34	1.08	0.55
M 43-15	3.84	0.77	0.76	0.42	0.32	0.60
M 43-85	3.36	2.56	2.48	1.86	1.51	0.80
M 50-00	3.31	0.00	0.00	0.00	0.00	0.60
M 50-50	3.52	2.38	1.69*	1.05*	0.62*	0.55
M 50-100	3.27	3.34	3.30	2.82	2.35	0.55
M 57-15	2.62	0.58	0.32	0.16	0.13	0.60
M 57-85	3.27	2.44	2.36	1.76	1.11	0.95
M 60-50	2.54	1.17	1.07	0.76	0.50	1.00

Table 4. Parameters for the characteristic tensile stress-strain curves

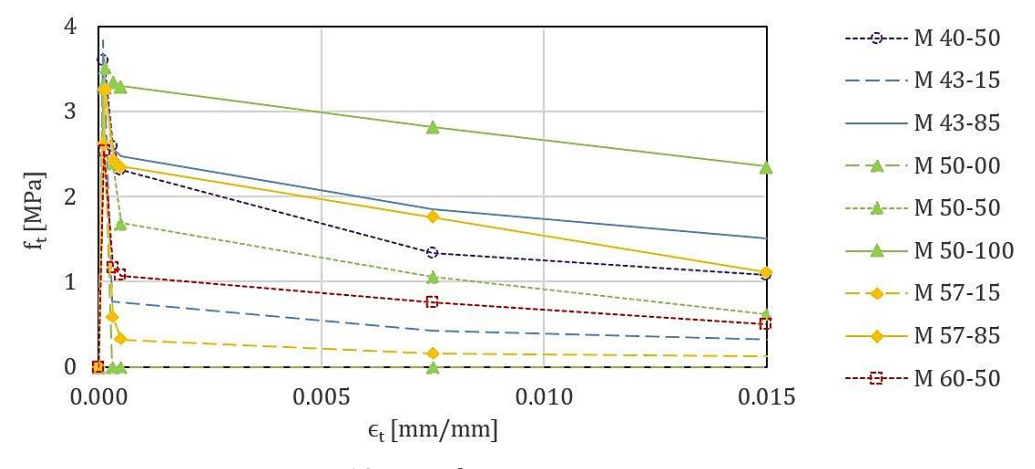


Fig.13. Tensile stress-strain curves

3.4 Experimental and Numerical Flexural Behavior

Figure 14 presents pictures of the FPBT and NLFEA results. The fracture process was captured by the model in an implicit manner through the decrease down to zero of the tensile capacity after the post-peak tensile behavior. There, the bridging effect of fibers is evident as the beam with %F=0.00 completely fractures (Figure 10a), contrary to the beam with fibers added (Figure 10b). The NLFEA exhibits strain concentration occurring at the fractured zone of the beam (Figure 10c) and also satisfactorily simulates the deformed configuration (Figure 10d).

Figure 15 presents the load vs. mid-span deflection curves obtained experimentally and through NLFEA. Due to illumination conditions and the duration time of the experiments, it was only possible to carry out DIC measurements for half of the FPBT (dashed thin lines). For the other half, only the peak load is reported (solid thin lines). The difference between experimental peak loads for beams with equal dosage of SFRSCC evidences the high statistical scatter in the mechanical response, mainly related to the random orientation and position of fibers. Nonetheless, the models had good accuracy to predict the maximum mean loads.

The initial linear portion of the experimental and NLFEA (solid thick lines) curves have a good agreement, however, in some cases (M 40-50, M 43-85 and M 57-85) the experimental results

exhibit a hardening behavior after this linear portion while the NLFEA tend to a softening behavior. This could be explained as described in Section 3.3, since the post linear-elastic behavior is controlled by the tensile constitutive relation, markedly influenced by the fibers. Proposals of other researchers achieve better post-cracking performances, nonetheless their tensile constitutive relationships were directly calibrated from bending tests and did not consider the statistical scatter (35,57).

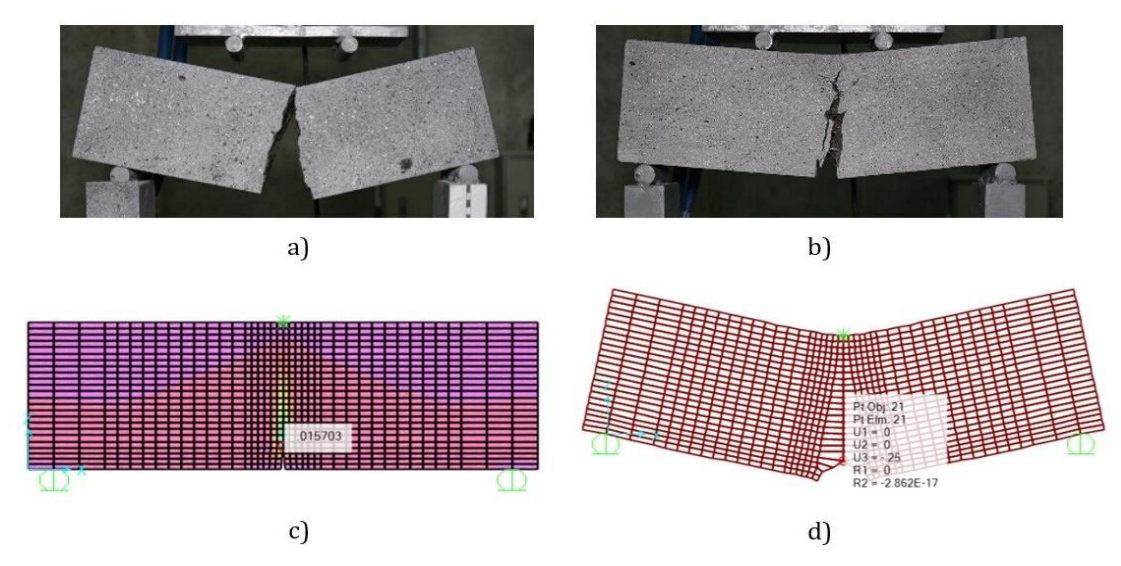
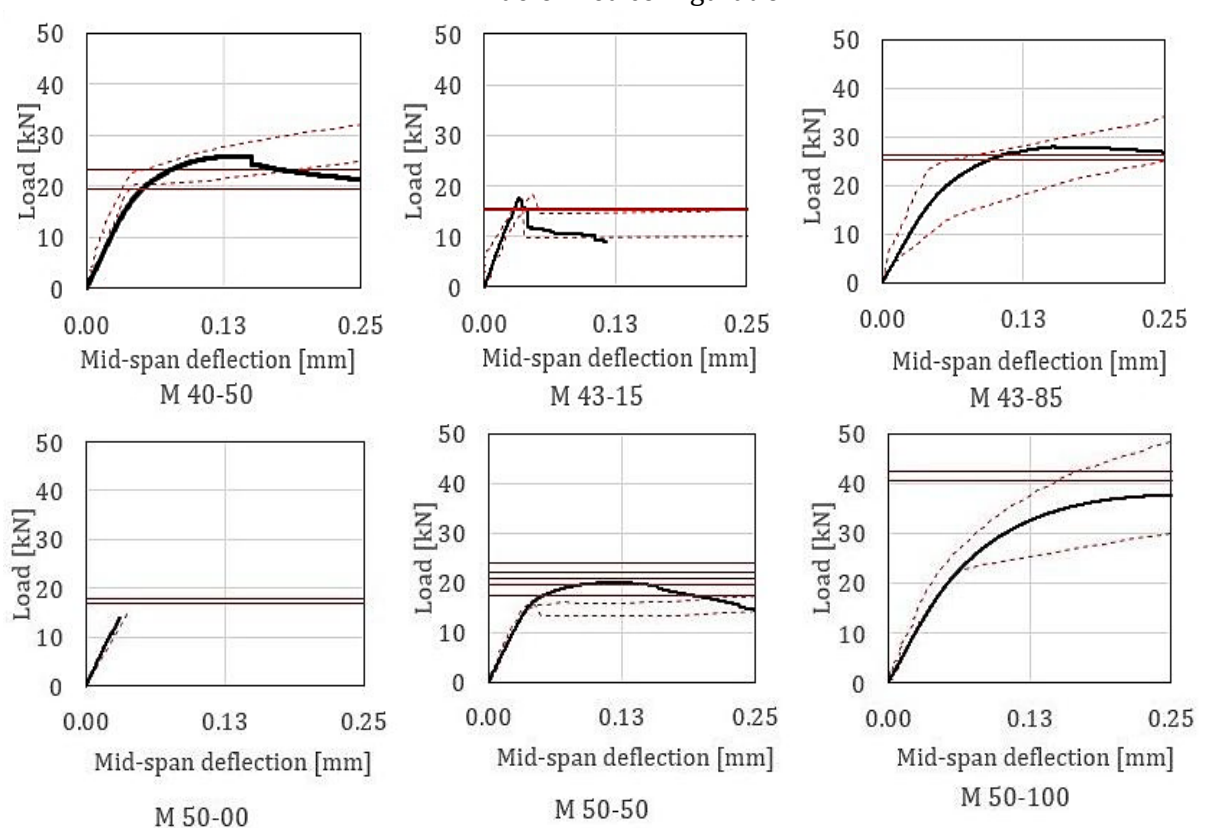


Fig. 14. SFRSCC beams on a) FPBT %F=0.00, b) FPBT %F=0.50, c) NLFEA strain field and d) NLFEA deformed configuration



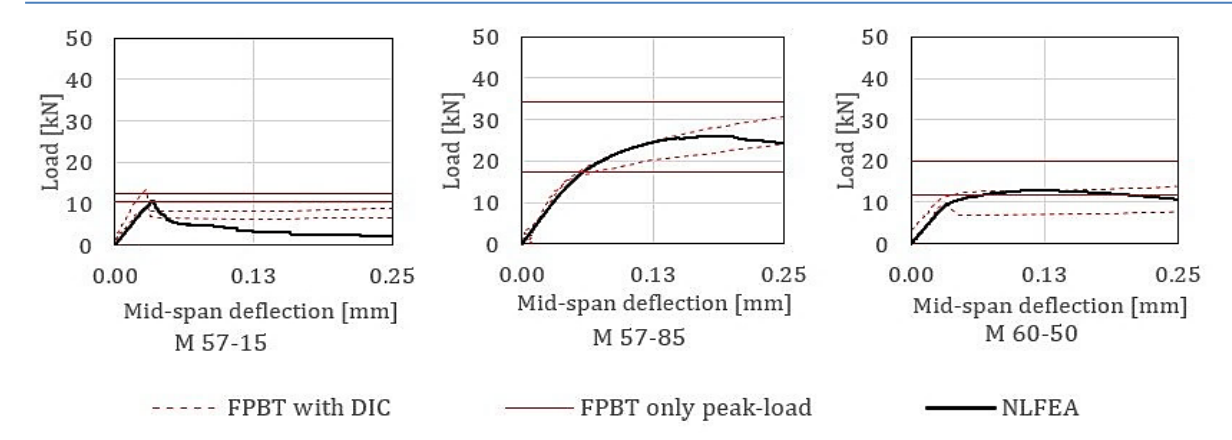


Fig. 15. Load-mid-span deflection curves

Table 5. Maximum bending moments

Mix	M _u - Tests average	M _u - NLFEA	Relative error
Mix -	[N-m]	[N-m]	%
M 40-50	1857.93	1945.65	4.72
M 43-15	1245.62	1314.00	5.49
M 43-85	2063.68	2094.75	1.51
M 50-00	1181.11	1050.60	11.05
M 50-50	1492.45	1502.63	0.68
M 50-100	3020.57	2822.78	6.55
M 57-15	856.77	801.45	6.46
M 57-85	1986.93	1950.83	1.82
M 60-50	1037.68	972.08	6.32

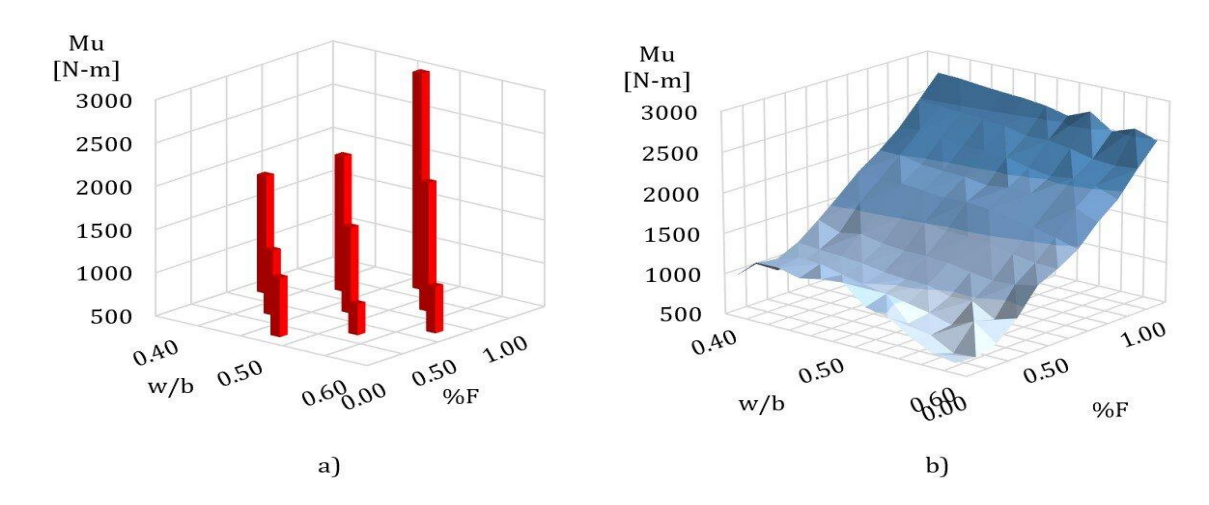


Fig.16. Surface plots of the maximum bending moment vs. w/b, %F a) Experimental test results, and b) NLFEA results

Table 6. Maximum bending moments for ANN training

NIO	w/b	0/ E	M_{u}	t	NIO	/b	0/ E	$M_{\rm u}$	t	NIO	/h	0/ E	M_{u}	t
N°	w/b	%F	[N-m]	[min]	N°	w/b	%F	[N-m]	[min]	N°	w/b	%F	[N-m]	[min]
1	0.46	0.40	1265	6	42	0.58	0.80	2024	5	83	0.42	0.90	2464	5
2	0.40	0.20	1050	11	43	0.40	0.90	2475	5	84	0.48	1.00	2661	5
3	0.50	0.30	1039	14	44	0.54	0.00	977	7	85	0.50	0.70	1868	6
4	0.54	0.80	2026	5	45	0.58	0.50	1332	6	86	0.58	0.90	2197	5
5	0.42	1.00	2739	5	46	0.54	0.40	1174	8	87	0.48	0.50	1504	6
6	0.46	0.90	2418	5	47	0.48	0.40	1240	5	88	0.42	0.50	1570	5
7	0.44	1.00	2707	5	48	0.40	0.80	2202	5	89	0.56	0.50	1375	12

	0.50	4.00	2550	_	40	0.50	0.00	04.4	0	0.0	0.50	4.00	2556	4.4
8	0.52	1.00	2559	5	49	0.58	0.30	814	8	90	0.58	1.00	2576	11
9	0.48	0.20	997	23	50	0.52	0.90	2331	6	91	0.56	0.90	2220	6
10	0.58	0.20	882	6	51	0.56	0.20	768	7	92	0.54	0.20	846	8
11	0.42	0.30	1141	14	52	0.44	0.30	1129	9	93	0.58	0.00	670	6
12	0.60	0.40	1207	14	53	0.50	0.80	2137	5	94	0.54	0.50	1437	6
13	0.46	0.10	1270	5	54	0.52	0.20	883	14	95	0.46	0.30	1102	11
14	0.52	0.70	1902	5	55	0.52	0.80	2068	6	96	0.54	0.10	808	6
15	0.54	0.30	959	10	56	0.42	0.80	2243	5	97	0.54	1.00	2670	7
16	0.40	0.70	1992	5	57	0.46	0.50	1528	5	98	0.50	0.20	947	6
17	0.50	1.00	2626	5	58	0.44	0.40	1319	9	99	0.58	0.40	1152	10
18	0.40	0.10	1069	7	59	0.56	0.70	1844	5	100	0.50	0.90	2329	5
19	0.40	0.50	1588	5	60	0.58	0.70	1840	6	101	0.48	0.70	1914	5
20	0.44	0.20	1036	20	61	0.58	0.10	582	11	102	0.42	0.00	1240	9
21	0.48	0.10	1203	6	62	0.44	0.70	1944	5	103	0.50	0.10	1134	6
22	0.42	0.40	1272	5	63	0.50	0.60	1743	10	104	0.44	0.00	1243	7
23	0.60	0.30	895	9	64	0.44	0.80	2206	5	105	0.46	1.00	2681	5
24	0.60	0.80	1924	6	65	0.56	0.60	1620	6	106	0.40	0.40	1370	13
25	0.58	0.60	1558	9	66	0.56	1.00	2484	6	107	0.50	0.00	1259	5
26	0.52	0.30	1032	15	67	0.54	0.70	1889	5	108	0.50	0.40	1240	5
27	0.54	0.60	1668	6	68	0.52	0.10	1103	19	109	0.42	0.60	1781	6
28	0.40	0.00	1001	8	69	0.46	0.80	2160	5	110	0.52	0.50	1462	5
29	0.56	0.40	1135	6	70	0.46	0.20	1016	18	111	0.48	0.60	1733	5
30	0.42	0.20	1039	30	71	0.44	0.50	1552	5	112	0.44	0.90	2445	5
31	0.56	0.30	974	6	72	0.50	0.50	1465	5	113	0.48	0.00	1234	7
32	0.40	0.30	1168	15	73	0.60	0.70	1727	6	114	0.60	0.60	1476	6
33	0.42	0.10	1057	30	74	0.42	0.70	2005	5	115	0.48	0.80	2157	6
34	0.48	0.90	2390	7	75	0.52	0.60	1716	5	116	0.44	0.60	1784	5
35	0.46	0.60	1761	6	76	0.52	0.00	1026	5	117	0.60	0.10	605	5
36	0.60	0.50	1325	11	77	0.40	1.00	2754	5	118	0.52	0.40	1219	5
37	0.60	0.90	2222	7	78	0.46	0.00	1179	5	119	0.48	0.30	1060	9
38	0.60	1.00	2490	13	79	0.46	0.70	1924	5	120	0.40	0.60	1816	7
39	0.60	0.00	628	5	80	0.44	0.10	1286	6	121	0.56	0.80	2060	6
40	0.56	0.10	734	28	81	0.54	0.90	2286	6		3.00	3.00		ŭ
41	0.60	0.20	677	24	82	0.56	0.00	806	7					
-11	0.00	5.20	0,,	4 1	02	5.55	3.00	000						

Using the peak loads, values of M_u were calculated as presented in Table 5. As expected, increasing the %F augmented the flexural capacity in all cases. Moreover, the predictive capacity of the numerical model is justified as the differences between the experimental and NLFEA bending moments are 5% on average, where better prediction occurs for the cases with fibers addition. With the validated NLFEAs, several simulations for the training of the ANNs were executed, as shown in Table 6. Their results are ordered based on a random permutation as required for assessing the ANNs. The total time of the simulations was 16.26 hours. Average computing time was 8 minutes, with some mixes requiring 30 minutes to achieve convergence.

The fact that only one structural element is modeled remarks the high computational cost needed to model nonlinear behavior of SFRSCC in commercial software. Furthermore, more computing time was required for beams with %F<0.30. This might be caused by the more brittle behavior of these mixtures, which leads to a sudden loss of stiffness after cracking occurs and may slow convergence in the numerical solution (e.g., M 43-15 and M 60-50 in Figure 15). A comparison of the NLFEA data with the experimental bending moments (Table 5) is presented in Figure 16. There it is noticeable how the tendency of the NLFEA models resemblance the experimental resultants and the marked effect that %F has on the flexural strength.

3.5 Bending Moment Predictions by ANNs

Convergence curves for the best run of each training algorithm for the ANNs with less weights (HL=1, HN=2) and more weights (HL=2, HN=20) are presented in Figure 17. As seen in all these graphs, no divergence occurs between the training and calibration curves, indicating no overfitting of the ANNs, as explained in (46). In general, MBP required more iterations to converge than PSO and GSA. This is explained as only one candidate solution is evaluated per iteration at MBP.

Moreover, PSO performed better at early iterations and converged faster (between 100 and 200 iterations) than GSA (between 400 and 500 iterations). Nonetheless, after these iterations, GSA keep identifying better solutions, which relates to a good exploitation capacity.

PSO successfully located minima in the early stages of the iterations despite the number of the ANNs weights, as the shape of the convergence curve is similar for HL=1, HN=2, and HL=2, HN=20, while MBP and GSA required more iterations to achieve convergence for the ANNs that required calculating more weights (HL=2, HN=20). Nevertheless, GSA achieved the best optimization for six of the eight different architectures of ANNs, as depicted in Table 7.

The MSE presented was calculated, including training, calibration, and validation data. Also, the coefficient of determination R² is presented as an additional measure of the fitness of the ANNs predicted bending moments to the NLFEA simulations (Table 6). The only scenarios where the MBP and PSO performed better than GSA were those with a higher number of weights (HL=2, HN=10 and HL=2, HN=20).

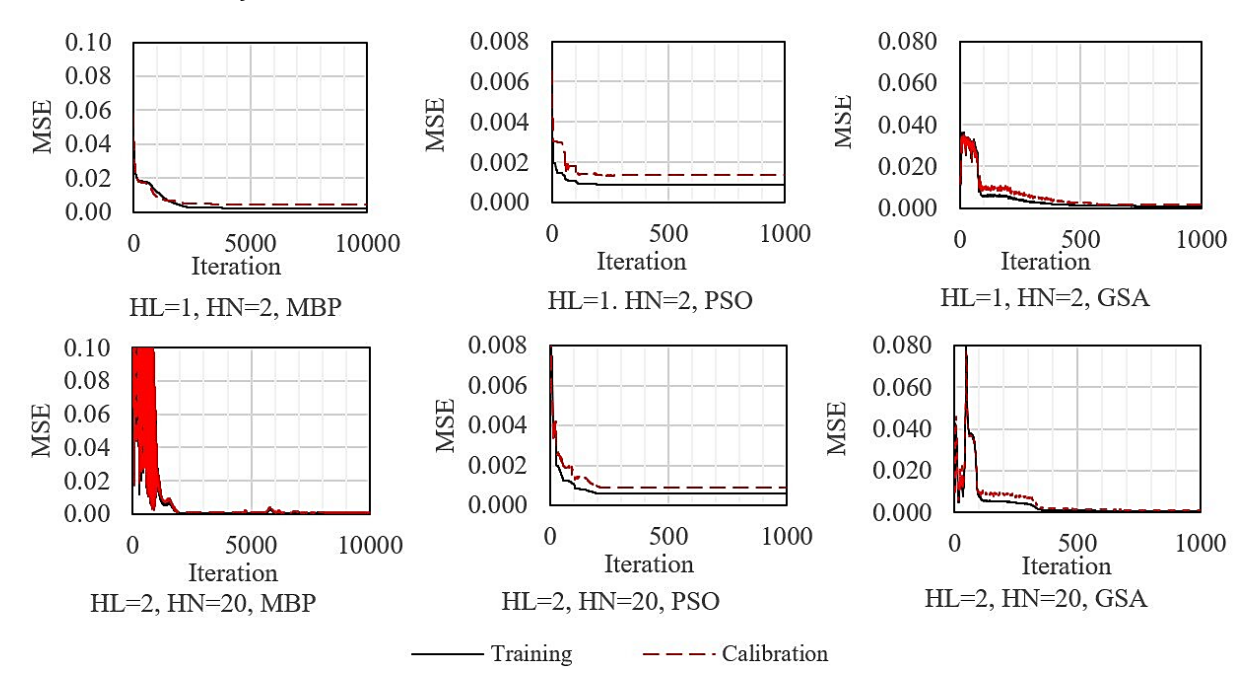


Fig.17. Convergence curves from the training and calibration of the ANN

Table 7. Be	est ANNs	results
-------------	----------	---------

HL	HN	Method	Training time [min]	MSE	R ²
1	2	GSA	7.20	1.00E-03	0.9728
1	5	GSA	7.65	4.19E-04	0.9887
1	10	GSA	8.52	3.57E-04	0.9904
1	20	GSA	10.05	5.38E-04	0.9857
2	2	GSA	17.62	6.71E-04	0.9818
2	5	GSA	24.47	4.20E-04	0.9887
2	10	PSO	42.85	3.71E-04	0.9899
2	20	MBP	14.30	5.08E-04	0.9941

The evidence from the convergence curves showed that GSA requires many iterations to achieve its best performance. Hence, a higher number of iterations may allow it to achieve better results for this ANNs architectures. By comparison of MSE and R², it was concluded that the ANN architecture that obtained the best predictions of bending moment was HL=1, HN=10, and trained with the GSA. The results of weights for this are presented in Table 8.

Weights between w/b and HL	Weights between %F and HL	Weights between HL and M_{u}	Biases HL	Bias M _u
0.560	-1.068	-0.770	-0.260	2.509
0.033	-0.514	0.247	0.437	
-0.529	-0.290	0.702	0.049	
-0.033	0.688	0.452	-0.073	
-0.623	0.461	0.821	0.933	
-0.042	0.617	-0.192	0.487	
0.667	1.226	0.424	-0.013	
0.129	0.356	0.687	-1.445	
0.316	0.416	0.703	-1.099	
-0.912	0.823	1.824	-3.384	

Prediction of M_u by means of the ANN are presented in Figure 18a. In general, the tendency of the ANN M_u is close to the experimental and NLFEA results (Figure 16). In addition, Figure 18b presents a contour lines map of the relative error of M_u (in percentage) between the results of the AAN and the NLFEA (Figure 16). There it can be depicted that relative errors are below 5% for most values of w/b and %F, nonetheless for %F<0.30 there are differences up to 20%, which may be improved in future research by using more training data in the assessment of neural networks for low fiber content.

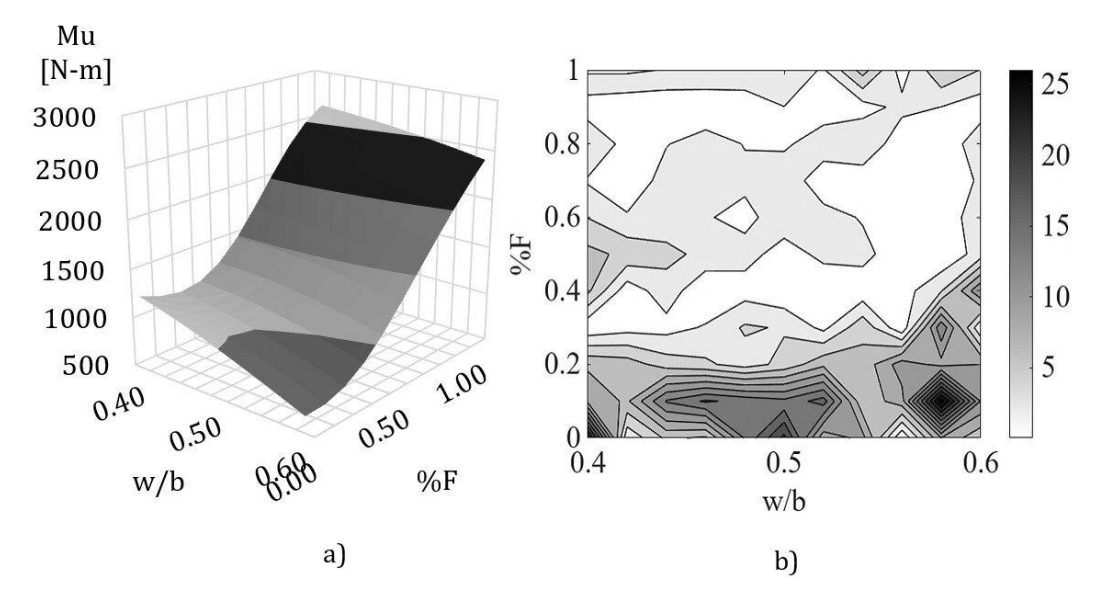


Fig. 18. a) Maximum bending moment with ANN and b) Contour of relative error between ANN and NLFEA results

4. Conclusions

The present research assessed the maximum bending moment of steel fiber reinforced self-compacting concrete beams, integrating uniaxial compression tests, indirect double punching Barcelona tests, four-point bending tests, constitutive modeling, non-linear finite element analysis, and artificial neural networks. The prediction of the flexural resistance was achieved for beams with water-binder ratios from 0.40 to 0.60 and steel hooked-ended fibers content percentages from 0.00% to 1.00% in volume. From the results, the following conclusions are withdrawn:

 Compressive strength can diminish in ranges from 2% to 18% when steel fibers are added, as supported by the uniaxial compression tests. Nonetheless, the post-peak deformation capacity and control of cracking due to compressive loads are improved.

- Tensile cracking strength is not markedly affected by the addition of fibers; however, higher amounts of fibers significantly improve the deformation capacity, strain ductility, and energy dissipation capacity in ranges from 20% to 280%.
- The tensile constitutive model from Barcelona tests presented here is an improvement from the original model. Nonetheless, the model still underestimates the post-peak stress capacity of the material. This is positive in terms of security related to design but is a disadvantage if precise predictions of the material behavior are required.
- The two-parameter Weibull distribution is a proper alternative to assess the characteristic values of mechanical properties of steel fiber self-compacting reinforced concrete since the experimental results had a better fit (in terms of P-values) compared to the normal distribution.
- Non-linear finite element analysis is feasible to predict the flexural capacity of fiber reinforced concrete beams. However, more computing time is required for low quantities of fibers. This might be caused by the abrupt changes in stress and stiffness after the peak load that occurs in brittle materials, which tends to slow the convergence and diminish the accuracy of numerical solutions.
- The gravitational search algorithm is an excellent alternative to train artificial neural networks for predicting the mechanical behavior of fiber concrete, as it reached mean squared errors lower than the classic algorithms, moment back-propagation, and particle swarm optimization.
- Artificial neural networks trained with experimentally calibrated finite element simulations can accurately predict (R²=0.99) the flexural resistance of beams with fiber reinforced concrete. However, more training data for low values of fibers might be used to improve its overall prediction capacity.

Acknowledgments

This research was financially supported by the Grupo de Investigación en Materiales de Construcción y Estructuras (INME) and the Universidad Industrial de Santander (UIS) in Colombia.

References

- [1] Wang L, Zhou H, Zhang J, Wang Z, Zhang L, Nehdi ML. Prediction of concrete strength considering thermal damage using a modified strength-maturity model. Constr Build Mater. 2023 Oct 12;400. https://doi.org/10.1016/j.conbuildmat.2023.132779
- [2] Ding Y, Zhang F, Torgal F, Zhang Y. Shear behaviour of steel fibre reinforced self-consolidating concrete beams based on the modified compression field theory. Compos Struct. 2012 Jul;94(8):2440-9. https://doi.org/10.1016/j.compstruct.2012.02.025
- [3] Meng G, Gao B, Zhou J, Cao G, Zhang Q. Experimental investigation of the mechanical behavior of the steel fiber reinforced concrete tunnel segment. Constr Build Mater. 2016 Nov 15;126:98-107. https://doi.org/10.1016/j.conbuildmat.2016.09.028
- [4] Sonebi M, Cevik A, Grünewald S, Walraven J. Modelling the fresh properties of self-compacting concrete using support vector machine approach. Constr Build Mater. 2016 Mar 1;106:55-64. https://doi.org/10.1016/j.conbuildmat.2015.12.035
- [5] Okamura H, Ouchi M. Self-Compacting Concrete. Vol. 1, Journal of Advanced Concrete Technology. 2003. https://doi.org/10.1016/B978-075065686-3/50295-0
- [6] El-Dieb AS, Reda Taha MM. Flow characteristics and acceptance criteria of fiber-reinforced self-compacted concrete (FR-SCC). Constr Build Mater. 2012 Feb;27(1):585-96. https://doi.org/10.1016/j.conbuildmat.2011.07.004
- [7] Altun F, Haktanir T, Ari K. Effects of steel fiber addition on mechanical properties of concrete and RC beams. Constr Build Mater. 2007 Mar;21(3):654-61. https://doi.org/10.1016/j.conbuildmat.2005.12.006
- [8] Batson GB, Birkimer DL, Burnett E, Gray BH, Henry R, Hoff GC, et al. State-of-the-Art Report on Fiber Reinforced Concrete. 1973.
- [9] Shakya K, Watanabe K, Matsumoto K, Niwa J. Application of steel fibers in beam-column joints of rigid-framed railway bridges to reduce longitudinal and shear rebars. Constr Build Mater. 2012 Feb;27(1):482-9. https://doi.org/10.1016/j.conbuildmat.2011.07.016
- [10] Rai B, Kumar S, Satish K. Influence of Water Binder Ratio and Chemical Admixture on the Properties of Self-Compacting Concrete with composite Cement-Fly Ash binder. Sustainable Structure and Materials [Internet]. 2019;2(1):97-117. Available from: https://doi.org/10.26392/SSM.2019.02.01.097

- [11] Gencel O, Brostow W, Datashvili T, Thedford M. Workability and mechanical performance of steel fiber-reinforced self-compacting concrete with fly ash. Compos Interfaces. 2011;18(2):169-84. https://doi.org/10.1163/092764411X567567
- [12] Fernandes PAL, Veludo J, Almeida N, Baptista J, Rodrigues H. Study of a self-compacting fiber-reinforced concrete to be applied in the precast industry. Innovative Infrastructure Solutions. 2018 Dec 1;3(1). https://doi.org/10.1007/s41062-018-0136-5
- [13] Mohamed N, Soliman AM, Nehdi ML. Mechanical performance of full-scale precast steel fibre-reinforced concrete pipes. Eng Struct. 2015 Feb 1;84:287-99. https://doi.org/10.1016/j.engstruct.2014.11.033
- [14] Nematollahi B, Voo YL, Saifulnaz M. R R. Structural behavior of precast Ultra-High Performance Fiber Reinforced Concrete (UHPFRC) cantilever retaining walls: Part II Full scale experimental testing. KSCE Journal of Civil Engineering. 2014;18(5):1481-95. https://doi.org/10.1007/s12205-014-0412-7
- [15] Niwa J, Shakya K, Matsumoto K, Watanabe K. Experimental Study on the Possibility of Using Steel Fiber-Reinforced Concrete to Reduce Conventional Rebars in Beam-Column Joints. Journal of Materials in Civil Engineering. 2012 Dec;24(12):1461-73. https://doi.org/10.1061/(ASCE)MT.1943-5533.0000536
- [16] La Comisión Asesora Permanente para el Régimen de Construcciones Sismo Resistentes. Reglamento Colombiano de Construcción Sismo-Resistente (NSR-10). Bogotá; 2010.
- [17] Moradi M, Bagherieh AR, Esfahani MR. Constitutive modeling of steel fiber-reinforced concrete. International Journal of Damage Mechanics. 2020 Mar 1;29(3):388-412. https://doi.org/10.1177/1056789519851159
- [18] Lee MK, Barr BIG. A four-exponential model to describe the behaviour of fibre reinforced concrete. Vol. 37. https://doi.org/10.1007/BF02481583
- [19] Huo L, Bi J, Zhao Y, Wang Z. Constitutive model of steel fiber reinforced concrete by coupling the fiber inclining and spacing effect. Constr Build Mater. 2021 Apr 19;280. https://doi.org/10.1016/j.conbuildmat.2021.122423
- [20] Blanco A, Pujadas P, Cavalaro S, De La Fuente A, Aguado A. Constitutive model for fibre reinforced concrete based on the Barcelona test. Cem Concr Compos. 2014;53:327-40. https://doi.org/10.1016/j.cemconcomp.2014.07.017
- [21] Chopra P, Sharma RK, Kumar M. Prediction of Compressive Strength of Concrete Using Artificial Neural Network and Genetic Programming. Advances in Materials Science and Engineering. 2016;2016. https://doi.org/10.1155/2016/7648467
- [22] Hodhod H, Abdeen MAM. Simulation and prediction for the effect of natural and steel fibers on the performance of concrete using experimental analyses and artificial neural networks numerical modeling. KSCE Journal of Civil Engineering. 2011 Nov;15(8):1373-80. https://doi.org/10.1007/s12205-011-1053-8
- [23] Paegle I, Minelli F, Fischer G. Cracking and load-deformation behavior of fiber reinforced concrete: Influence of testing method. Cem Concr Compos. 2016 Oct 1;73:147-63. https://doi.org/10.1016/j.cemconcomp.2016.06.012
- [24] Bencardino F. Mechanical parameters and post-cracking behaviour of hpfrc according to three-point and four-point bending test. Advances in Civil Engineering. 2013;2013. https://doi.org/10.1155/2013/179712
- [25] Bencardino F, Rizzuti L, Spadea G, Swamy RN. Implications of test methodology on post-cracking and fracture behaviour of Steel Fibre Reinforced Concrete. Compos B Eng. 2013;46:31-8. https://doi.org/10.1016/j.compositesb.2012.10.016
- [26] Montgomery D, Runger G. Applied Statistics and Probability for Engineers. Fifth. John Wiley & Sons Inc, editor. Rosewood Drive, Danvers, USA: John Wiley & Sons Inc; 2011.
- [27] European Project Gruop. The European Guidelines for Self-Compacting Concrete Specification, Production and Use [Internet]. 2005. Available from: www.efnarc.org
- [28] Quiceno Pérez V, Cotes Prieto D, Zapata Orduz LE. Mechanical characterization of self-compacting steel fiber reinforced concrete using digital image correlation. Eng Fract Mech. 2021 Apr 1;246. https://doi.org/10.1016/j.engfracmech.2021.107618
- [29] Soutsos M, Hatzitheodorou A, Kanavaris F, Kwasny J. Compressive Strength Estimates of Adiabatically Cured Concretes Using Maturity Methods. Journal of Materials in Civil Engineering. 2019 Jul;31(7). https://doi.org/10.1061/(ASCE)MT.1943-5533.0002757
- [30] American Society for Testing Materials. ASTM C39 Standard Test Method for Compressive Strength of Cylindrical Concrete Specimens [Internet]. 2019. Available from: www.astm.org,
- [31] Asociación Española de Normalización y Certificación (AENOR). UNE 83515-Concreto reforzado con fibras. Determinación de la resistencia a fisuración, tenacidad y resistencia residual a tracción. Método Barcelona [Internet]. Madrid; 2010. Available from: www.aenor.es
- [32] International Union of Laboratories and Experts in Construction Materials S and S (RILEM). RILEM TC 162-TDF: Test and design methods for steel fibre reinforced concrete. 2000.

- [33] American Society for Testing Materials. ASTM C1609 Standard Test Method for Flexural Performance of Fiber-Reinforced Concrete (Using Beam With Third-Point Loading) [Internet]. Available from: www.astm.org
- [34] Wang T, Zhao H, Hao J, Zu J. Research on compressive stress Strain relationship of fiber reinforced concrete. In: Advanced Materials Research. 2011. p. 384-92. https://doi.org/10.4028/www.scientific.net/AMR.168-170.384
- [35] Laranjeira De Oliveira F, Aguado De Cea A. Design-oriented constitutive model for steel fiber reinforced concrete. 2010.
- [36] Bortolotti L. Double-Punch Test for Tensile and Compressive Strengths in Concrete. 1988;
- [37] International Federation for Structural Concrete (fib). Model code for concrete structures 2010. Berlin: Wilhelm Ernst & Sohn; 2010.
- [38] Zapata-Ordúz LE, Portela G, Suárez OM. Weibull statistical analysis of splitting tensile strength of concretes containing class F fly ash, micro/nano-SiO2. Ceram Int. 2014 Jun;40(5):7373-88. https://doi.org/10.1016/j.ceramint.2013.12.083
- [39] Deng B, Jiang D, Gong J. Is a three-parameter Weibull function really necessary for the characterization of the statistical variation of the strength of brittle ceramics? J Eur Ceram Soc. 2018 Apr 1;38(4):2234-42. https://doi.org/10.1016/j.jeurceramsoc.2017.10.017
- [40] MathWorks. MATLAB R 2020a. MatWorks; 2020.
- [41] Computers & Structures (CSI). SAP2000. 2022.
- [42] Computers&Structures Inc. CSI Analysis Reference Manual [Internet]. 2016. Available from: www.csiamerica.com
- [43] Adhikary BB, Mutsuyoshi H. Prediction of shear strength of steel fiber RC beams using neural networks. Constr Build Mater. 2006 Nov;20(9):801-11. https://doi.org/10.1016/j.conbuildmat.2005.01.047
- [44] Minitab LLC. Minitab V.16. 2016.
- [45] Açikgenç M, Ulaş M, Alyamaç KE. Using an Artificial Neural Network to Predict Mix Compositions of Steel Fiber-Reinforced Concrete. Arab J Sci Eng. 2015 Feb 1;40(2):407-19. https://doi.org/10.1007/s13369-014-1549-x
- [46] Du KL, Swamy MNS. Neural networks and statistical learning. Vol. 9781447155713, Neural Networks and Statistical Learning. Springer-Verlag London Ltd; 2014. 1-824. https://doi.org/10.1007/978-1-4471-5571-3
- [47] Mashhadban H, Kutanaei SS, Sayarinejad MA. Prediction and modeling of mechanical properties in fiber reinforced self-compacting concrete using particle swarm optimization algorithm and artificial neural network. Constr Build Mater. 2016 Aug 30;119:277-87. https://doi.org/10.1016/j.conbuildmat.2016.05.034
- [48] Awolusi TF, Oke OL, Akinkurolere OO, Sojobi AO, Aluko OG. Performance comparison of neural network training algorithms in the modeling properties of steel fiber reinforced concrete. Heliyon [Internet]. 2018;e01115. https://doi.org/10.1016/j.heliyon.2018.e01115
- [49] Kennedy J, Eberhart R. Particle Swarm Optimization. IEEE. 1995;
- [50] Rashedi E, Nezamabadi-pour H, Saryazdi S. GSA: A Gravitational Search Algorithm. Inf Sci (N Y). 2009 Jun 13;179(13):2232-48. https://doi.org/10.1016/j.ins.2009.03.004
- [51] Khajehzadeh M, Raihan Taha M, El-Shafie A, Eslami M. Optimization of Shallow Foundation Using Gravitational Search Algorithm. Research Journal of Applied Sciences Engineering and Technology [Internet]. 2012;4(9):1124-30. https://www.researchgate.net/publication/230996869
- [52] Pajak M, Ponikiewski T. Flexural behavior of self-compacting concrete reinforced with different types of steel fibers. Vol. 47, Construction and Building Materials. 2013. p. 397-408. https://doi.org/10.1016/j.conbuildmat.2013.05.072
- [53] Larsen IL, Thorstensen RT. The influence of steel fibres on compressive and tensile strength of ultra high performance concrete: A review. Vol. 256, Construction and Building Materials. Elsevier Ltd; 2020. https://doi.org/10.1016/j.conbuildmat.2020.119459
- [54] Molins C, Aguado A, Saludes S. Double punch test to control the energy dissipation in tension of FRC (Barcelona test). Materials and Structures/Materiaux et Constructions. 2009 May;42(4):415-25. https://doi.org/10.1617/s11527-008-9391-9
- [55] ACI Committee 214., American Concrete Institute. Guide to evaluation of strength test results of concrete. American Concrete Institute; 2011. 16 p.
- [56] Tumidajski PJ, Fiore L, Khodabocus T, Lachemi M, Pari R. Comparison of Weibull and normal distributions for concrete compressive strengths. Canadian Journal of Civil Engineering. 2006 Oct;33(10):1287-92. https://doi.org/10.1139/106-080
- [57] Campione G, Letizia Mangiavillano M. Fibrous reinforced concrete beams in flexure: Experimental investigation, analytical modelling and design considerations. Eng Struct. 2008 Nov;30(11):2970-80. https://doi.org/10.1016/j.engstruct.2008.04.019

Appendix 1

MATLAB script for calibration of the Weibull parameters

```
%1. Barcelona
%2. Compression
for ensayo=2:2
 ini=4; fin=71;
 fini=int2str(ini): ffin=int2str(fin):
 switch ensayo
   case 1
      tic()
      aa='barcelona par3.xlsx';
      sesion=xlsread(aa,'DATOS',strcat('B',fini,':','B',ffin));
      zz='Modelos constitutivos corr.xlsx';
      consti=xlsread(aa,'DATOS',strcat('U',fini,':','AD',ffin));
      e1=consti(:,1); s1=consti(:,2);
      e2=consti(:,3); s2=consti(:,4);
      e3=consti(:,5); s3=consti(:,6);
      e4=consti(:,7); s4=consti(:,8);
      e5=consti(:,9); s5=consti(:,10);
      cont1=1;
      cont2=1;
      for i=1:4:(fin-ini+1)
        if sesion(i)==1 \mid | sesion(i)==2 \mid | sesion(i)==5 \mid | ...
         sesion(i)==7 \mid sesion(i)==13
         e11(cont1:cont1+3)=e1(i:i+3); s11(cont1:cont1+3)=s1(i:i+3);
         e21(cont1:cont1+3)=e2(i:i+3); s21(cont1:cont1+3)=s2(i:i+3);
         e31(cont1:cont1+3)=e3(i:i+3); s31(cont1:cont1+3)=s3(i:i+3);
         e41(cont1:cont1+3)=e4(i:i+3); s41(cont1:cont1+3)=s4(i:i+3);
         e51(cont1:cont1+3)=e5(i:i+3); s51(cont1:cont1+3)=s5(i:i+3);
         cont1=cont1+4;
        else
          e12(cont2:cont2+3)=e1(i:i+3); s12(cont2:cont2+3)=s1(i:i+3);
         e22(cont2:cont2+3)=e2(i:i+3); s22(cont2:cont2+3)=s2(i:i+3);
         e32(cont2:cont2+3)=e3(i:i+3); s32(cont2:cont2+3)=s3(i:i+3);
         e42(cont2:cont2+3)=e4(i:i+3); s42(cont2:cont2+3)=s4(i:i+3);
         e52(cont2:cont2+3)=e5(i:i+3); s52(cont2:cont2+3)=s5(i:i+3);
          cont2=cont2+4;
        end
      end
      s11(s11==0)=0.00000000001; s21(s21==0)=0.0000000001;
      s31(s31==0)=0.00000000001; s41(s41==0)=0.0000000001;
      s51(s51==0)=0.0000000001;
      s12(s12==0)=0.00000000001; s22(s22==0)=0.0000000001;
      s32(s32==0)=0.00000000001; s42(s42==0)=0.0000000001;
      s52(s52==0)=0.0000000001;
      Wpare11=wblfit(e11);
      dist=makedist('Weibull','A',Wpare11(1),'B',Wpare11(2));
      [ho,PvalueWe11]=adtest(e11,'Distribution',dist);
      Wpars11=wblfit(s11);
      dist=makedist('Weibull','A',Wpars11(1),'B',Wpars11(2));
      [ho,PvalueWs11]=adtest(s11,'Distribution',dist);
      avge11=mean(e11); stde11=std(e11);
```

```
avgs11=mean(s11); stds11=std(s11);
Wpare21=wblfit(e21);
dist=makedist('Weibull','A',Wpare21(1),'B',Wpare21(2));
[ho,PvalueWe21]=adtest(e21,'Distribution',dist);
Wpars21=wblfit(s21);
dist=makedist('Weibull','A',Wpars21(1),'B',Wpars21(2));
[ho,PvalueWs21]=adtest(s21,'Distribution',dist);
avge21=mean(e21); stde21=std(e21);
avgs21=mean(s21); stds21=std(s21);
Wpare31=wblfit(e31);
dist=makedist('Weibull','A',Wpare31(1),'B',Wpare31(2));
[ho,PvalueWe31]=adtest(e31,'Distribution',dist);
Wpars31=wblfit(s31);
dist=makedist('Weibull','A',Wpars31(1),'B',Wpars31(2));
[ho,PvalueWs31]=adtest(s31,'Distribution',dist);
avge31=mean(e31); stde31=std(e31);
avgs31=mean(s31); stds31=std(s31);
Wpare41=wblfit(e41);
dist=makedist('Weibull','A',Wpare41(1),'B',Wpare41(2));
[ho.PvalueWe41]=adtest(e41,'Distribution',dist);
Wpars41=wblfit(s41);
dist=makedist('Weibull','A',Wpars41(1),'B',Wpars41(2));
[ho,PvalueWs41]=adtest(s41,'Distribution',dist);
avge41=mean(e41); stde41=std(e41);
avgs41=mean(s41); stds41=std(s41);
Wpare51=wblfit(e51);
dist=makedist('Weibull','A',Wpare51(1),'B',Wpare51(2));
[ho,PvalueWe51]=adtest(e51,'Distribution',dist);
Wpars51=wblfit(s51);
dist=makedist('Weibull','A',Wpars51(1),'B',Wpars51(2));
[ho,PvalueWs51]=adtest(s51,'Distribution',dist);
avge51=mean(e51); stde51=std(e51);
avgs51=mean(s51); stds51=std(s51);
cont=0;
for i=1:4:size(s12,2)
  cont=cont+1;
 Wpare12(cont,:)=wblfit(e12(i:i+3));
  dist=makedist('Weibull','A',Wpare12(cont,1),'B',Wpare12(cont,2));
  [ho,PvalueWe12(cont)]=adtest(e12(i:i+3),'Distribution',dist);
  Wpars12(cont,:)=wblfit(s12(i:i+3));
  dist=makedist('Weibull','A',Wpars12(cont,1),'B',Wpars12(cont,2));
 [ho,PvalueWs12(cont)]=adtest(s12(i:i+3),'Distribution',dist);
 avge12(cont)=mean(e12(i:i+3)): stde12(cont)=std(e12(i:i+3)):
  avgs12(cont)=mean(s12(i:i+3)); stds12(cont)=std(s12(i:i+3));
  Wpare22(cont,:)=wblfit(e22(i:i+3));
  dist=makedist('Weibull','A',Wpare22(cont,1),'B',Wpare22(cont,2));
  [ho,PvalueWe22(cont)]=adtest(e22(i:i+3),'Distribution',dist);
  Wpars22(cont,:)=wblfit(s22(i:i+3));
  dist=makedist('Weibull','A',Wpars22(cont,1),'B',Wpars22(cont,2));
  [ho,PvalueWs22(cont)]=adtest(s22(i:i+3),'Distribution',dist);
  avge22(cont)=mean(e22(i:i+3)); stde22(cont)=std(e22(i:i+3));
 avgs22(cont)=mean(s22(i:i+3)); stds22(cont)=std(s22(i:i+3));
 Wpare32(cont,:)=wblfit(e32(i:i+3));
  dist=makedist('Weibull','A',Wpare32(cont,1),'B',Wpare32(cont,2));
```

```
[ho,PvalueWe32(cont)]=adtest(e32(i:i+3),'Distribution',dist);
   Wpars32(cont,:)=wblfit(s32(i:i+3));
   dist=makedist('Weibull','A',Wpars32(cont,1),'B',Wpars32(cont,2));
   [ho,PvalueWs32(cont)]=adtest(s32(i:i+3),'Distribution',dist);
   avge32(cont)=mean(e32(i:i+3)); stde32(cont)=std(e32(i:i+3));
   avgs32(cont)=mean(s32(i:i+3)); stds32(cont)=std(s32(i:i+3));
   Wpare42(cont,:)=wblfit(e42(i:i+3));
   dist=makedist('Weibull','A',Wpare42(cont,1),'B',Wpare42(cont,2));
   [ho,PvalueWe42(cont)]=adtest(e42(i:i+3),'Distribution',dist);
   Wpars42(cont,:)=wblfit(s42(i:i+3));
   dist=makedist('Weibull','A',Wpars42(cont,1),'B',Wpars42(cont,2));
   [ho,PvalueWs42(cont)]=adtest(s42(i:i+3),'Distribution',dist);
   avge42(cont)=mean(e42(i:i+3));
   stde42(cont)=std(e42(i:i+3));
   avgs42(cont)=mean(s42(i:i+3));
   stds42(cont)=std(s42(i:i+3));
   Wpare52(cont,:)=wblfit(e52(i:i+3));
   dist=makedist('Weibull','A',Wpare52(cont,1),'B',Wpare52(cont,2));
   [ho,PvalueWe52(cont)]=adtest(e52(i:i+3),'Distribution',dist);
   Wpars52(cont,:)=wblfit(s52(i:i+3));
   dist=makedist('Weibull','A',Wpars52(cont,1),'B',Wpars52(cont,2));
    [ho,PvalueWs52(cont)]=adtest(s52(i:i+3),'Distribution',dist);
   avge52(cont)=mean(e52(i:i+3));
   stde52(cont)=std(e52(i:i+3));
   avgs52(cont)=mean(s52(i:i+3));
   stds52(cont)=std(s52(i:i+3));
  Wpare1=[Wpare11;Wpare12]; PvalueWe1=[PvalueWe11,PvalueWe12]';
  Wpars1=[Wpars11;Wpars12]; PvalueWs1=[PvalueWs11,PvalueWs12]';
  avge1=[avge11,avge12]'; stde1=[stde11,stde12]';
  avgs1=[avgs11,avgs12]'; stds1=[stds11,stds12]';
  Wpare2=[Wpare21;Wpare22]; PvalueWe2=[PvalueWe21,PvalueWe22]';
  Wpars2=[Wpars21;Wpars22]; PvalueWs2=[PvalueWs21,PvalueWs22]';
  avge2=[avge21,avge22]'; stde2=[stde21,stde22]';
  avgs2=[avgs21,avgs22]'; stds2=[stds21,stds22]';
  Wpare3=[Wpare31;Wpare32]; PvalueWe3=[PvalueWe31,PvalueWe32]';
  Wpars3=[Wpars31;Wpars32]; PvalueWs3=[PvalueWs31,PvalueWs32]';
  avge3=[avge31,avge32]'; stde3=[stde31,stde32]';
  avgs3=[avgs31,avgs32]'; stds3=[stds31,stds32]';
  Wpare4=[Wpare41;Wpare42]; PvalueWe4=[PvalueWe41,PvalueWe42]';
  Wpars4=[Wpars41;Wpars42]; PvalueWs4=[PvalueWs41,PvalueWs42]';
  avge4=[avge41,avge42]'; stde4=[stde41,stde42]';
  avgs4=[avgs41,avgs42]'; stds4=[stds41,stds42]';
  Wpare5=[Wpare51;Wpare52]; PvalueWe5=[PvalueWe51,PvalueWe52]';
  Wpars5=[Wpars51;Wpars52]; PvalueWs5=[PvalueWs51,PvalueWs52]';
  avge5=[avge51,avge52]'; stde5=[stde51,stde52]';
  avgs5=[avgs51,avgs52]'; stds5=[stds51,stds52]';
case 2
  aa='compresion par.xlsx':
 sesion=xlsread(aa,'DATOS',strcat('B',fini,':','B',ffin));
 zz='Modelos Constitutivos.xlsx';
  fc=xlsread(aa,'DATOS',strcat('V',fini,':','V',ffin));
  Ec=xlsread(aa,'DATOS',strcat('AI',fini,':','AI',ffin));%Modulo tangente
  cont1=1;
  cont2=1:
  for i=1:4:(fin-ini+1)
   if sesion(i)==1 \mid | sesion(i)==2 \mid | sesion(i)==5 \mid | ...
       sesion(i)==7 || sesion(i)==13
     fc1(cont1:cont1+3)=fc(i:i+3);
     Ec1(cont1:cont1+3)=Ec(i:i+3);
```

```
cont1=cont1+4;
       else
         fc2(cont2:cont2+3)=fc(i:i+3);
         Ec2(cont2:cont2+3)=Ec(i:i+3);
         cont2=cont2+4;
       end
     end
     Wpar1=wblfit(fc1);
     dist=makedist('Weibull','A',Wpar1(1),'B',Wpar1(2));
     [ho,pvalue]=adtest(fc1,'Distribution',dist);
     PvalueW1=pvalue; Wpar1E=wblfit(Ec1);
     dist=makedist('Weibull','A',Wpar1E(1),'B',Wpar1E(2));
     [ho,pvalue]=adtest(Ec1,'Distribution',dist);
     PvalueW1E=pvalue;
     avgfc1=mean(fc1); stdfc1=std(fc1);
     avgEc1=mean(Ec1); stdEc1=std(Ec1);
     cont=0;
     for i=1:4:size(fc2,2)
       cont=cont+1;
       param=wblfit(fc2(i:i+3)); Wpar2(cont,:)=param;
       dist=makedist('Weibull','A',Wpar2(cont,1),'B',Wpar2(cont,2));
       [ho,pvalue]=adtest(fc2(i:i+3),'Distribution',dist);
       PvalueW2(cont)=pvalue;
       param=wblfit(Ec2(i:i+3)); Wpar2E(cont,:)=param;
       dist=makedist('Weibull','A',Wpar2E(cont,1),'B',Wpar2E(cont,2));
       [ho,pvalue]=adtest(Ec2(i:i+3),'Distribution',dist);
       PvalueW2E(cont)=pvalue;
       avgfc2(cont)=mean(fc2(i:i+3)); stdfc2(cont)=std(fc2(i:i+3));
       avgEc2(cont)=mean(Ec2(i:i+3)); stdEc2(cont)=std(Ec2(i:i+3));
     Wpar=[Wpar1;Wpar2]; PvalueW=[PvalueW1,PvalueW2]';
     WparE=[Wpar1E;Wpar2E]; PvalueWE=[PvalueW1E,PvalueW2E]';
     avgfc=[avgfc1,avgfc2]'; stdfc=[stdfc1,stdfc2]';
     avgEc=[avgEc1,avgEc2]'; stdEc=[stdEc1,stdEc2]';
   otherwise
 end
end
Appendix 2
MATLAB script for automation of SAP2000
clear;
clc;
ini=62; fin=121;
Datosred=zeros(1010,(fin-ini+1)*2);
for i=1:(fin-ini+1)
 %1. Define which SAP to use: already open one (true) o new one (false)
 if i==1
   EnesteSAP=false();
 else
   EnesteSAP=false();
 %2. Specify SAP file route (true) otherwise the last used SAP file route will be used.
 EspecificarSAP=true();
 %3. Specify SAP file route.
 DireccionSAP='C:\Program Files\Computers and Structures\SAP2000 22\SAP2000.exe';
 %4. Specify the route of the API to use.
```

DireccionAPIDLL='C:\Program Files\Computers and Structures\SAP2000 22\SAP2000v1.dll';

```
%5. Specify the route of the file where the model is located
  DireccionCarpetaModelo='E:\David\Documentos\Estructuras\MAESTRÍA EN INGENIERÍA CIVIL\Vigas
SFRSCC_SAP\Red neural';
 if ~exist(DireccionCarpetaModelo, 'dir') %If the file exists use it, otherwise create it
   mkdir(DireccionCarpetaModelo);
  end
 NombreModelo=strcat(int2str(ini-1+i),'.sdb'); %Name of the model
  DireccionModelo=strcat(DireccionCarpetaModelo,filesep,NombreModelo); %Text to route
 %6. Create the API assistent.
  a=NET.addAssembly(DireccionAPIDLL):
  asistenteAPI=SAP2000v1.Helper;
  asistenteAPI=NET.explicitCast(asistenteAPI,'SAP2000v1.cHelper');
  %7. Open SAP or use one already open.
  if EnesteSAP
   SapObject=asistenteAPI.GetObject('CSI.SAP2000.API.SapObject');
   SapObject=NET.explicitCast(SapObject,'SAP2000v1.cOAPI');
 else
   if EspecificarSAP
     SapObject=asistenteAPI.CreateObject(DireccionSAP);
     SapObject=asistenteAPI.CreateObjectProgID('CSI.SAP2000.API.SapObject');
   SapObject = NET.explicitCast(SapObject,'SAP2000v1.cOAPI');
   SapObject.ApplicationStart;
 asistenteAPI=0;
  %8.Create SAP model
  SapModel=NET.explicitCast(SapObject.SapModel,'SAP2000v1.cSapModel');
  ret=SapModel.InitializeNewModel;
 %9. Open the SAP model.
  File=NET.explicitCast(SapModel.File,'SAP2000v1.cFile');
  ret=File.OpenFile(DireccionModelo);
 tic()
  %15. Run the SAP model.
 Analyze=NET.explicitCast(SapModel.Analyze,'SAP2000v1.cAnalyze');
 ret=Analyze.RunAnalysis();
 AnalysisResults=NET.explicitCast(SapModel.Results,'SAP2000v1.cAnalysisResults');
 AnalysisResultsSetup=NET.explicitCast(AnalysisResults.Setup,'SAP2000v1.cAnalysisResultsSetup');
  ret=AnalysisResultsSetup.DeselectAllCasesAndCombosForOutput;
  ret=AnalysisResultsSetup.SetCaseSelectedForOutput("FPT-Cracking");
 ret=AnalysisResultsSetup.SetOptionNLStatic(2);
 NumberResults=0:
  Obj=NET.createArray('System.String',1010);
 Elm=NET.createArray('System.String',1010);
 ACase=NET.createArray('System.String',1010);
  StepType=NET.createArray('System.String',1010);
  StepNum=NET.createArray('System.Double',1010);
  U1=NET.createArray('System.Double',1010); U2=NET.createArray('System.Double',1010);
  U3=NET.createArray('System.Double',1010); R1=NET.createArray('System.Double',1010);
 R2=NET.createArray('System.Double',1010); R3=NET.createArray('System.Double',1010);
[ret,NumberResults,Obj,Elm,ACase,StepType,StepNum,U1,U2,U3,R1,R2,R3]=AnalysisResults.JointDispl("21"
```

,SAP2000v1.eItemTypeElm.ObjectElm,...

```
NumberResults, Obj, Elm, ACase, StepType, StepNum, U1, U2, U3, R1, R2, R3);
 for j=1:NumberResults
   Desplazamiento(j)=U3(j)*-1000;
 NumberResults=0:
 StepType=NET.createArray('System.String',1010);
 StepNum=NET.createArray('System.Double',1010);
 LoadCase=NET.createArray('System.String',1010);
 Fx=NET.createArray('System.Double',1); Fy=NET.createArray('System.Double',1);
 Fz=NET.createArray('System.Double',1); Mx=NET.createArray('System.Double',1);
 My=NET.createArray('System.Double',1); Mz=NET.createArray('System.Double',1);
 gx=0; gy=0; gz=0;
[ret,NumberResults,LoadCase,StepType,StepNum,Fx,Fy,Fz,Mx,My,Mz,gx,gy,gz]=AnalysisResults.BaseReact(
NumberResults,LoadCase,StepType,StepNum,...
   Fx,Fy,Fz,Mx,My,Mz,gx,gy,gz);
 for j=1:NumberResults
   Carga(j)=Fz(j);
 end
 NumberResults=0:
 StepType=NET.createArray('System.String',1010);
 StepNum=NET.createArray('System.Double',1010);
 LoadCase=NET.createArray('System.String',1010);
 GD=NET.createArray('System.String',1010);
 DType=NET.createArray('System.String',1);
 Numbdat(i)=NumberResults;
 %17. Close SAP
   ret=SapModel.SetModelIsLocked(false());
   ret=SapObject.ApplicationExit(false());
   File=0:
   PropMaterial=0; PropFrame=0;
   FrameObj=0; AreaObj=0;
   PointObj=0; View=0;
   LoadPatterns=0; Analyze=0;
   AnalysisResults=0:
   AnalysisResultsSetup=0;
   SapModel=0; SapObject=0;
   tiempo(2*i-1:2*i)=[toc()/60,0];
   Datosred(1:length(Desplazamiento),2*i-1:2*i)=[Desplazamiento',Carga'];
   clear Desplazamiento Carga
end
xlswrite('Curvas ajustadas final.xlsx',Datosred,'Datos red neural','DT40')
```

xlswrite('Curvas ajustadas final.xlsx',tiempo,'Datos red neural','DT38')